DESY HERA 93-10

Fermilab Library
0 1160 0049184 9

NAME | I.D No. | M.S.
RETURN TO FERMILAB LIBRARY

45

DESY HERA 93-10
October 1993

Emittance Growth in Proton Storage Rings due to the Combined Effect of Non-Linear Fields and Modulation Effects with more than one Frequency

O. Brüning

Deutsches Elektronen-Synchrotron DESY
Hamburg, Germany

FERMILAB
OCT 18 1995
LIBRARY

DESY behält sich alle Rechte für den Fall der Schutzrechtserteilung und für die wirtschaftliche Verwertung der in diesem Bericht enthaltenen Informationen vor.

DESY reserves all rights for commercial use of information included in this report, especially in case of filing application for or grant of patents.

Emittance Growth in Proton Storage Rings due to the Combined Effect of Non-Linear Fields and Modulation Effects with more than one Frequency.

O. Brüning

Deutsches Elektronen-Synchrotron (DESY),
Notkestrasse 85, W-2000 Hamburg 52, Germany

Abstract

Looking at the simple model structure of a long FODO cell with harmonic or random tune modulation, and non-linear fields, we calculate upper limits for the drift and diffusion coefficients as functions of the modulation frequencies and depths, and the phase space position. The analysis shows that the combined effect of slow and fast modulation frequencies leads to an enhanced emittance growth. Taking the modulation frequencies and the depths for the slow tune modulation as fixed parameters, we calculate upper limits for the modulation depths of the fast tune modulation as it might be generated by the imperfections in the power supplies. Furthermore, the analysis shows that the motion on the coupling resonance in combination with the beam-beam interaction leads to an additional tune modulation. Depending on the phase space position, the coupling resonance turns out to have either a stabilizing or destabilizing effect on the particle motion. The analytically calculated drift coefficients agree qualitatively as well as quantitatively with the tracking data. A comparison of the calculated drift coefficients with the ones measured in the HERA proton storage ring shows that the analyzed mechanism can at least in principle lead to drift and diffusion coefficients of the same order of magnitude as the ones measured in the HERA storage ring, and that excessive fluctuations in the power supply can limit the beam lifetime.

1 Introduction

In a previous paper [1] we presented a qualitative analysis of the emittance growth due to the combined effect of tune modulation and non-linear fields. We showed how a simultaneous tune modulation with more than one modulation frequency can lead to a much larger emittance growth than in the case of a tune modulation with only one frequency but the same net modulation depth. The results of our analysis agreed qualitatively with the 1991 SPS experiment [2]. A qualitative understanding of the processes underlying the increased emittance growth in the presence of more than one modulation frequency leads naturally to the question to what extent the existing diffusion models of nonlinear dynamics may be used for a quantitative analysis of the emittance growth. In [3] we started such a quantitative analysis of the diffusion processes by considering only one modulation frequency and looking at the stochastic pump diffusion [4][5] as the underlying mechanism for the emittance growth. The analysis showed that for a wide range of parameters the diffusion model could be successfully used to describe the emittance growth and that the diffusion due to the non-linear aspects of the particle motion can at least in principle lead to growth rates of the same order of magnitude as the ones observed in a real storage ring. However, the diffusion turned out to be limited to a small fraction of the accessible Q-space, so that the overall emittance growth of a large particle distribution is still small.

In this paper we extend the quantitative analysis of [3] to the case of a tune modulation with more than one modulation frequency and look at a harmonic as well as a random tune modulation. A numerical analysis of an explicitly stochastic tune modulation without any harmonic components was first presented by R. Brinkmann [6]. We will see that a harmonic tune modulation with slow and fast frequency components, or a harmonic fast tune modulation plus a random modulation, lead not only to diffusion and drift coefficients of the same order of magnitude as the ones measured in a real storage ring [7], but also to a diffusion which occurs over a large range of the accessible Q-space. Depending on the modulation frequencies and depths, the diffusion can be strong enough to limit the beam lifetime.

Even if the phase space volume occupied by the particles contains no low-order sum resonances for the un-modulated system, the modulation sidebands of a fast tune modulation might project the sum resonances into the phase space volume occupied by the particle distribution. An additional slow tune modulation leads to a set of closely spaced resonance sidebands about every sideband of the fast tune modulation. Below a critical slow modulation frequency the sidebands might overlap [5], producing a relatively broad region of phase space which supports chaotic motion. In the following we will call this region the 'modulational layer' according to [8]. The stochastic character of the motion inside the modulational layer provides a source for the particle diffusion even if the system has no explicitly stochastic modulation signal. If the slow modulation sidebands do not overlap, we observe no particle diffusion, unless we introduce an explicitly stochastic tune modulation. The analysis of the particle diffusion reveals four aspects of the emittance growth. First, we will see that the presence of more than one modulation frequency (harmonic or random changes in the tunes) might lead to relatively wide tune intervalls in which we observe an emittance growth. Second, depending on the modulation frequencies and depths, the particle diffusion occurs only in specific regions of the accessible phase space. For example, depending on the fast modulation frequencies and the tune values, one can support a particle diffusion only in the beam halo. This type of local particle diffusion can support a slow emittance growth in the

beam halo, and might be relevant for a parasitic experiment during the normal luminosity runs in HERA, such as the proposed HERA-B experiment[9]. However, in the case of more than one fast tune modulation frequency with non-vanishing modulation strength, or in the case of tune values close to the coupling resonance, the overlaping sidbands might lead to a particle diffusion over a large area of the phase space and the local character of the particle diffusion disappears. Third, depending on the phase space position, the motion on the coupling resonance can enhance or decrease the particle diffusion, and fourth, the diffusion due to the non-linear particle motion can be large enough to limit the beam lifetime.

In the following we will look at a model structure for the HERA proton storage ring with up to four horizontal tune modulation frequencies. We will look at a working point close to the coupling resonance and located between the 7th and 10th order sum resonances, as it was used in the 1992 HERA luminosity run. We choose the following linear Q-values: ($Q_{hor.} = 31.2971$; $Q_{vert.} \in [32.290, 32.299]$). The model structure consists of six transfer maps separated by four sextupole kicks, powered and placed in such a way as to reproduce the nonlinear detuning of the HERA proton storage ring, and two beam-beam kicks in the weak-strong approximation for round beams. For the fast tune modulation we consider a harmonic tune modulation with the two frequencies $1200Hz$ and $50Hz$, as they might occur in the current output of the HERA-p power supply due to the conversion of the a-c power lines into the d-c output signal [10][11]. For the slow tune modulation we look at a harmonic as well as a random change of the horizontal tune. For the harmonic slow tune modulation, we choose up to two frequencies in the range of $0.6Hz$ and $10Hz$ with a total root mean square (rms) modulation amplitude of $\Delta Q_{rms} \approx 3 \cdot 10^{-5}$, which is the upper bound for the rms modulation amplitude due to the ground motion in the HERA storage ring [12].

In a first step, we look at moderate modulation depths for the fast frequencies ($\Delta Q \approx 2.5 \cdot 10^{-4}$), as they might occur due to the design tolerances of the power supplies and assume a proton beam diameter which is larger than that of the electron beam. If the Q-values lie close the coupling resonance, the energy oscillations in the transverse phase space might have a stabilizing or destabilizing effect on the particle motion. If the particles lie inside the regions of regular motion around the stable fixed points of the coupling resonance, the effect of the coupling resonance is stabilizing, and if the particles are just outside the separatrix of the coupling resonance or inside the stochastic layer around the separatrix, the effect of the coupling resonance is destabilizing. In all cases, the analytical estimates of the emittance growth agree nicely with the numerical data of our computer simulations and are of the same order of magnitude as the measured drift velocities in the proton storage ring of HERA [7]. In a second step, we choose a larger modulation depths for the fast $1200Hz$ modulation ($\Delta Q \approx 1.25 \cdot 10^{-3}$), as it might occur due to a power supply of poor quality. With the large modulation amplitude, the particle diffusion occurs over a large fraction of the accessible phase space, and might limit the beam lifetime. At the end of our analysis we look at the local character of the particle diffusion. Depending on the modulation frequencies, the described diffusion mechanism can support an emittance growth only in specific regions of the accessible phase space.

The paper is organized as follows: First we present the Hamilton function and map for our model structure as it was derived in [3], and analyze the resonance sidebands caused by the fast tune modulation. In a second and third part, we introduce the tune modulation and discuss its effect on the phase space structure. In a fourth part, we look at the effect of the coupling resonance on the particle motion, and in a fifth part, we introduce the diffusion mechanism

and discuss the qualitative dependence of the diffusion on the Q-values, the modulation strengths, and the modulation frequencies. A comparison of the analytical estimates for the drift coefficients agrees qualitatively as well as quantitatively with the tracking data.

2 The Hamilton Function

The Hamilton function corresponding to our model structure was derived in detail in [3] and we will restrict ourself here to a short presentation. Introducing the potential for the sextupole kicks [13]

$$V_{sext}(x,z,s) = (\delta_{L_2}(s) + \delta_{L_3}(s) + \delta_{L_5}(s) + \delta_{L_6}(s)) \cdot \frac{\lambda}{6} \cdot (x^3 - 3xz^2), \tag{1}$$

the beam-beam kicks [14]

$$V_{beam-beam}(x,z,s) = (\delta_{L_1}(s) + \delta_{L_4}(s)) \cdot \xi \frac{4\pi\sigma^2}{\beta^*} \cdot \int_0^\infty \frac{1 - \exp\left[-\frac{(x-d_x)^2+(z-d_z)^2}{2\sigma^2+q}\right]}{2\sigma^2+q} dq \tag{2}$$

and a horizontal tune modulation with N frequencies, the Hamilton function can be written as

$$H = \nu_x \cdot \left[1 + \sum_{p=1}^{N} \frac{\Delta Q_p}{Q_x} \cdot \cos\left(\frac{2\pi\Omega_p}{L} \cdot s\right)\right] \cdot I_x + \nu_z \cdot I_z + V_{sext}(x,z,s) + V_{beam-beam}(x,z,s) \tag{3}$$

λ is the integrated sextupole strength ($\lambda = \frac{e}{P_0} \int_0^L \left(\frac{\partial^2 B_z}{\partial x^2}\right)_{x=z=0} ds \rightarrow [\lambda] = \frac{1}{m^2}$), B the magnetic field, e the unit charge, L the length of the model storage ring, P_0 the particle momentum, ΔQ_p the modulation depths, Ω_p the modulation frequencies in number of turns ($\rightarrow f_{mod}[Hz] = f_{rev}[Hz] \cdot \Omega$), ξ the beam-beam parameter, σ the electron beam size, β^* the beta function at the intersection points, d_x and d_z are the horizontal and vertical beam offsets respectively, and $\delta_{L_j}(s)$ are periodic delta functions ($\delta_{L_j}(s) = \sum_m \delta(s - m \cdot L_j)$). I_x and I_z are the canonical momenta of the action-angle variables for the linear system and are related to the Cartesian coordinates by

$$y = \sqrt{2\beta_y(s) I_y} \cdot \cos(\phi_y); \qquad \frac{dy}{ds} = -\sqrt{\frac{2I_y}{\beta_y(s)}} \cdot \sin(\phi_y); \qquad y = x, z. \tag{4}$$

In the following analysis we choose

$Q_x = 31.2971$	$\beta_x \approx 32m$	$L = 6.3 \cdot 10^3 m$	$P_0 = 820 GeV/c$
$Q_z \in [32.290; 32.299]$			$\beta_z \approx 31m$
$\xi = 0.0016$	$\beta^* = 32m$	$\sigma = 0.1mm$	$\lambda = 1.1m^{-2}$
$f_{rev} = 47.3KHz$		$d_x = 0.05mm$	$d_z = 0.0mm$
Position of the Sextupole Kicks			
$L_2 = 36.23m$	$L_3 = 1076.27m$	$L_5 = 5269.41m$	$L_6 = 6300.0m$
Position of the Beam-Beam Kicks			
$L_1 = 20.13m$		$L_4 = 3154.72m$,	

(5)

with $\nu_x = \frac{2\pi}{L} \cdot Q_x$ and $\nu_z = \frac{2\pi}{L} \cdot Q_z$. P_0c is the proton design energy for HERA and f_{rev} the proton revolution frequency. The phase space volume V_{beam} accessible to the particles inside the proton beam can be expressed in terms of the action-angle variables by

$$I_y \in [0.0m; 10.0 \cdot 10^{-9}m], \qquad \phi_y \in [-\pi; +\pi], \qquad y = x, z, \tag{6}$$

where the upper boundary for the action variables corresponds to a normalized emittance of $17 \cdot 10^{-6}m$.

Using Deprit perturbation theory [15][4] for the sextupole kicks and a Fast Fourier Transform (FFT) for the beam-beam kicks, we can calculate the Fourier representation of (3) with respect to the angle variables in (4) [3]. The analysis in [3] showed that the Fourier coefficients of the sextupole kicks are small compared to the beam-beam kicks as long as the particles stay within V_{beam}. Therefore, we will neglect the sextupole kicks in the following. Introducing the vectors $\vec{n}_{fast} = (n_1, n_2, ..., n_{N_1})$, $\vec{r}_{fast} = (r_1, r_2, ..., r_{N_1})$, $\vec{\Omega}_{fast} = (\Omega_1, \Omega_2, ..., \Omega_{N_1})$ for the fast modulation frequencies, $\vec{n}_{slow} = (n_{N_1+1}, n_{N_1+2}, ..., n_N)$, $\vec{r}_{slow} = (r_{N_1+1}, r_{N_1+2}, ..., r_N)$, and $\vec{\Omega}_{slow} = (\Omega_{N_1+1}, \Omega_{N_1+2}, ..., \Omega_N)$ for the slow frequencies, and eliminating the tune modulation from the linear part of (3), we get [3]:

$$H = H_{driving} + H_{coupling} \tag{7}$$

with

$$\begin{aligned} H_{driving} &= \nu_x \cdot I_x + \nu_z \cdot I_z + A_{0,0,0}(I_x, I_z) + \sum_{l,m,k,n_{slow}} \tilde{A}_{l,m,k,\vec{n}_{fast},\vec{n}_{slow}}(I_x, I_z) \times \\ &\cos\left(l\phi_x + m\phi_z + \frac{2\pi}{L}\left(k + \vec{n}_{fast} \cdot \vec{\Omega}_{fast} + \vec{n}_{slow} \cdot \vec{\Omega}_{slow}\right) s + \delta_{l,k}\right) \end{aligned} \tag{8}$$

$$\begin{aligned} H_{coupling} &= \sum_{r_{slow}} \tilde{A}_{2,-2,2,\vec{r}_{fast},\vec{r}_{slow}}(I_x, I_z) \cdot \\ &\cos\left(2\phi_x - 2\phi_z + \frac{2\pi}{L}\left(2 + \vec{r}_{fast} \cdot \vec{\Omega}_{fast} + \vec{r}_{slow} \cdot \vec{\Omega}_{slow}\right) s + \delta_{2,-2,2}\right). \end{aligned} \tag{9}$$

Here, we have introduced the notation

$$\tilde{A}_{l,m,k,\vec{n}_{fast},\vec{n}_{slow}} = \left[\prod_{p=1}^{N} J_{n_p}\left(\frac{l\Delta Q_p}{\Omega_p}\right)\right] \cdot A_{l,m,k}, \tag{10}$$

with $A_{l,m,k}$ being the mode amplitude of the un-modulated system, and $J_{n_p}\left(\frac{l\Delta Q_p}{\Omega_p}\right)$ being the Bessel functions of the first kind. From now on, we will characterize each resonance by the corresponding parameter vector $\vec{\alpha} = (l, m, k, \vec{n}_{fast}, \vec{n}_{slow})$.

In the following we will look at (8) as the driving term for the diffusion. If the slow tune modulation creates modulational layers around the beam-beam resonances in (8), the stochastic character of the horizontal motion will lead to particle diffusion.

The equation of motion corresponding to the linear part of the Hamilton function (3) can be integrated, yielding

$$\begin{aligned} I_z(s_0 + hL + \Delta L) &= I_z(s_0 + hL), \quad \phi_z(s_0 + hL + \Delta L) = \phi_z(s_0 + hL) + \Delta_z(\Delta L), \\ I_x(s_0 + hL + \Delta L) &= I_x(s_0 + hL), \quad \phi_x(s_0 + hL + \Delta L) = \phi_x(s_0 + hL) + \Delta_x(s_0 + hL, \Delta L), \end{aligned} \tag{11}$$

with

$$\begin{aligned} \Delta L &= L_{i+1} - L_i, \; i = 1,6, \; L_{6+1} = L_1, \\ \Delta_z(\Delta L) &= \nu_z \cdot \Delta L, \\ \Delta_x(s_0 + hL, \Delta L) &= \nu_x \Delta L + \sum_{p=1}^{N}\left[\frac{2\Delta Q_p}{\Omega_p}\sin\left(\frac{\pi\Omega_p\Delta L}{L}\right)\cos\left(2\pi\Omega_p h + \frac{\pi\Omega_p \cdot (2s_0 + \Delta L)}{L}\right)\right]. \end{aligned} \tag{12}$$

Taking into account the nonlinear kicks (2) and transforming back to the variables x, P_x, z, and P_z, the position after the $(h+1)^{th}$ passage through the model ring can be expressed as a function of the position after the hth passage through the model ring via a successive application of the linear transfer maps

$$\begin{pmatrix} \tilde{x} \\ \tilde{P}_x \\ \tilde{z} \\ \tilde{P}_z \end{pmatrix}_{s_0+h\cdot L+\Delta L} = \begin{pmatrix} \cos(\Delta_x) & \beta_x \cdot \sin(\Delta_x) & 0 & 0 \\ -\sin(\Delta_x)/\beta_x & \cos(\Delta_x) & 0 & 0 \\ 0 & 0 & \cos(\Delta_z) & \beta_z \cdot \sin(\Delta_z) \\ 0 & 0 & -\sin(\Delta_z)/\beta_z & \cos(\Delta_z) \end{pmatrix} \cdot \begin{pmatrix} x \\ P_x \\ z \\ P_z \end{pmatrix}_{s_0,h\cdot L}, \tag{13.a}$$

and the beam-beam kicks

$$\begin{pmatrix} \tilde{x} \\ \tilde{P}_x \\ \tilde{z} \\ \tilde{P}_z \end{pmatrix} = \begin{pmatrix} x \\ P_x \\ z \\ P_z \end{pmatrix} + \begin{pmatrix} 0 \\ -\frac{8\pi\sigma^2}{\beta^*} \cdot \xi \cdot \frac{x}{r^2} \cdot [1 - \exp(-r^2/2\sigma^2)] \\ 0 \\ -\frac{8\pi\sigma^2}{\beta^*} \cdot \xi \cdot \frac{z}{r^2} \cdot [1 - \exp(-r^2/2\sigma^2)] \end{pmatrix} \tag{13.b}$$

(with $r^2 = x^2 + z^2$) to the particle coordinates.

We will use this combined map for the construction of the surface of section (SoS) [4] for the horizontal particle motion ($I_z \equiv 0$, $\phi_z \equiv 0$) and for the tracking of particle distributions through our model structure. For the SoS, we choose the surface $mod(s, \kappa \cdot L) = 0$, with $\kappa \in \mathbb{Z}$ imposed by the map (13). For the construction of the SoS, one has to limit the tune modulation to frequencies that satisfy the resonance condition

$$\gamma + \vec{\delta} \cdot \vec{\Omega} = 0, \qquad \gamma, \delta_p \in \mathbb{Z}, \quad \mathrm{p} = 1, 2, .., \mathrm{N} \rightarrow \Omega_\mathrm{p} = \frac{\mathrm{q}}{\mathrm{r}}, \; \mathrm{q}, \mathrm{r} \in \mathbb{Z}. \tag{14}$$

Rather than taking the particle coordinates after each passage through the model storage ring, as in the case without tune modulation, we take the coordinates now only after each κth passage through the model ring, with κ being the smallest common denominator of the Ω_p. Without this restriction, we can only construct a stroboscobic phase space projection, which does not depict the clear resonance island structure.

3 Harmonic Tune Modulation

In this section we discuss the effect a the fast and slow tune modulation on the resonance structure of our model Hamiltonian. First, we describe the effects of the fast tune modulation and introduce the notion of seeding resonances, and second, we discuss the effects of an additional slow tune modulation.

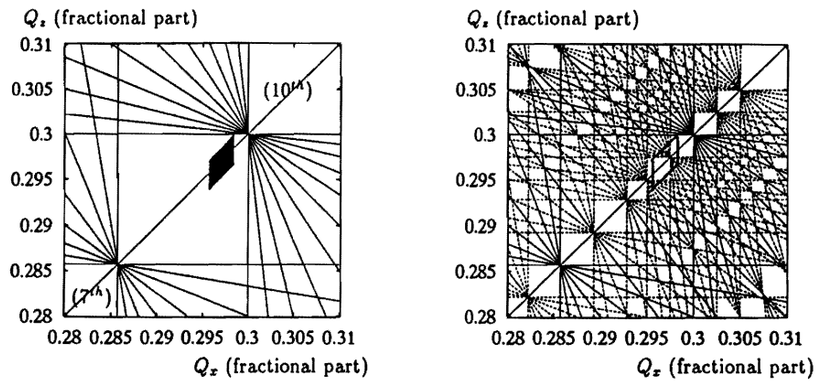

Figure 1: The particle distribution in the transverse Q-diagram.
Left: The resonance lines up to 10th order in x and z without any tune modulation.
Right: The resonance lines and their sidebands for a fast tune modulation with $1200Hz$.

3.1 Fast Tune Modulation

Without any tune modulation, the phase space volume occupied by the particles (V_{beam} given by (6)) contains no low-order sum resonances and the fixed point equations

$$\frac{\partial H}{\partial I} = 0; \qquad \frac{\partial H}{\partial \phi} = 0 \tag{15}$$

have no solutions for $(I_x, I_z) \in V_{beam}$, except for the solutions of the coupling mode. The left-hand side of Fig.1 shows a proton distribution in the transverse Q-space, as it was used in the 1992 luminosity run for HERA-p. The particles are located in the direct neighbourhood of the coupling resonance, between the 7th and 10th order sum resonances. The Q-diagram shows the horizontal and vertical resonances up to 10th order in x and z. Without tune modulation, the particles do not lie on any low-order sum resonances.

This situation changes if we take the tune modulation into consideration. Using the canonical transformation

$$\begin{aligned}
F_2 &= \hat{I}_{res} \cdot \left(l \cdot \phi_x + m \cdot \phi_z + \frac{2\pi}{L} \cdot \left[k + \vec{n}_{fast} \cdot \vec{\Omega}_{fast} + \vec{n}_{slow} \cdot \vec{\Omega}_{slow} \right] s \right) + \\
&\quad \hat{I}_- \cdot (l \cdot \phi_x - m \cdot \phi_z), \\
I_x &= l \cdot \hat{I}_{res} + l \cdot \hat{I}_-, \qquad I_z = m \cdot \hat{I}_{res} - m \cdot \hat{I}_-, \\
\phi_x &= \frac{\hat{\phi}_{res} + \hat{\phi}_-}{2l} - \frac{2\pi}{2lL} \cdot \left[k + \vec{n}_{fast} \cdot \vec{\Omega}_{fast} + \vec{n}_{slow} \cdot \vec{\Omega}_{slow} \right] s, \\
\phi_z &= \frac{\hat{\phi}_{res} - \hat{\phi}_-}{2m} - \frac{2\pi}{2mL} \cdot \left[k + \vec{n}_{fast} \cdot \vec{\Omega}_{fast} + \vec{n}_{slow} \cdot \vec{\Omega}_{slow} \right] s,
\end{aligned} \tag{16}$$

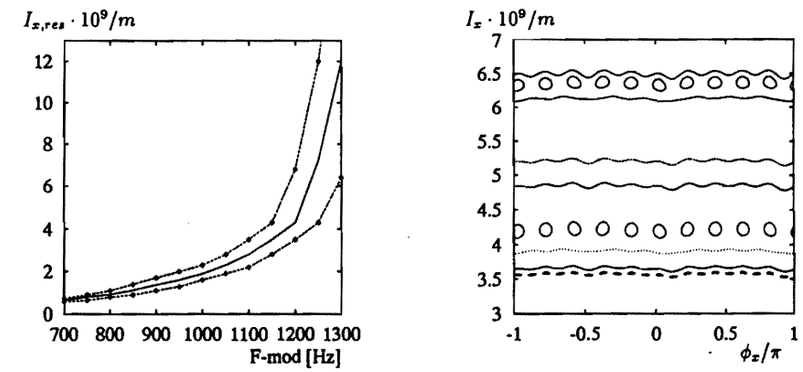

Figure 2: The position of the seeding sidebands for the horizontal $(10, 0, -313)$ mode and the parameter values (5).
Left: The position as a function of the modulation frequency. The solid line shows the position of the $(f_1 = 1200Hz, n_1 = 1, f_2 = 50Hz, n_2 = 0)$ seeding resonance, and the lines with dots show the positions of the lower and upper $50Hz$ sidebands: $(f_1 = 1200Hz, n_1 = 1, f_2 = 50Hz, n_2 = \pm 1)$.
Right: The corresponding resonance islands in the surface of action for $I_z \equiv 0$ and $\Delta Q_{1200Hz} = 1.25 \cdot 10^{-4}$.

and looking at the single resonance approximation for the horizontal driving term

$$\begin{aligned}
H_{driving} &= \hat{I}_{res} \left[l\nu_x + m\nu_z + \frac{2\pi}{L} \cdot \left(k + \vec{n}_{fast} \cdot \vec{\Omega}_{fast} \right) + \vec{n}_{slow} \cdot \vec{\Omega}_{slow} \right] + \\
&\quad \hat{I}_- \left[l\nu_x - m\nu_z \right] + A_{0,0,0} \left(\hat{I}_{res}, \hat{I}_- \right) + \tilde{A}_{l,m,k,\vec{n}_{fast},\vec{n}_{slow}} \left(\hat{I}_x, \hat{I}_- \right) \cdot \cos \left(\hat{\phi}_{res} + \delta\phi_{l,0,k} \right),
\end{aligned} \tag{17}$$

we can rewrite the fixed point equations for the resonance as

$$\left(l \cdot \nu_x + m \cdot \nu_z + \frac{2\pi}{L} \left(k + \vec{n}_{fast} \cdot \vec{\Omega}_{fast} + \vec{n}_{slow} \cdot \vec{\Omega}_{slow} \right) \right) + \left(\frac{\partial \tilde{A}_{0,0,0}}{\partial \hat{I}_{res}} \left(\hat{I}_{res}, \hat{I}_- \right) + \frac{\partial \tilde{A}_{l,m,k}}{\partial \hat{I}_{res}} \left(\hat{I}_{res}, \hat{I}_- \right) \right) = 0 \tag{18}$$

$$\sin \left(\hat{\phi}_{res} + \delta\phi_{l,0,k} \right) = 0. \tag{19}$$

The fast tune modulation leads to a set of additional fixed points, each corresponding to a sideband of the fast frequency modulation. We characterize each sideband by the modulation frequencies and the order of the sidebands

$$(f_1, n_1, f_2, n_2, ..., f_{N_1}, n_{N_1}). \tag{20}$$

For a fast tune modulation, the modulation sidebands might not overlap, but reach into the phase space volume V_{beam}. In this case, the fixed point equations (18) have solutions for

$(I_x, I_z) \in V_{beam}$ and the particle motion might lie on a non-linear resonance. According to [3], we call these modulation sidebands seeding resonances, as they form the seeds for a chaotic region due to an additional slow tune modulation. The right-hand side of Fig.1 shows the Q-diagram for the same particle distribution as in the left-hand side of Fig.1, but with the resonance sidebands of a fast tune modulation with $1200Hz$. One clearly recognizes the new resonance lines in the area covered by the particle distribution.

In the following analysis, we look at a fast tune modulation with

$$\begin{array}{|c|c|}\hline f_{fast,1} = 1200Hz \rightarrow \Omega_{fast,1} = 1/40 & \Delta Q_{fast,1} \in [1.25 \cdot 10^{-4},\ 1.25 \cdot 10^{-3}] \\ \hline f_{fast,2} = 50Hz \rightarrow \Omega_{fast,2} = 1/960 & \Delta Q_{fast,2} \in [0,\ 4.38 \cdot 10^{-4}] \\ \hline \end{array} \tag{21}$$

as it might occur due to the imperfections of the HERA-p power supplies [11].

The left-hand side of Fig.2 shows the position of the horizontal $(10, 0, -313)$ seeding resonances for $(I_z \equiv 0)$ as a function of the modulation frequency $[I_{x,res}(f_{fast})]$. The solid line shows the position of the $(f_1 = 1200Hz, n_1 = 1, f_2 = 50Hz, n_2 = 0)$ seeding resonance and the dashed lines with dots show the upper and lower $50Hz$ sidebands around the $1200Hz$ seeding resonance: $(f_1 = 1200Hz, n_1 = 1, f_2 = 50Hz, n_2 = \pm 1)$. As the fast modulation frequency increases, the seeding resonances move to larger I_x values and the $(f_1 = 1200Hz, n_1 = 1, f_2 = 50Hz, n_2 = \pm 1)$ seeding resonances move away from each other. In the right-hand side of Fig.2 we see the corresponding resonance islands for $\Delta Q_{1200Hz} = 1.25 \cdot 10^{-4}$ and $\Delta Q_{50Hz} = 3.13 \cdot 10^{-4}$ in the horizontal surface of section. The island chain in the middle corresponds to the $(f_1 = 1200Hz, n_1 = 1, f_2 = 50Hz, n_2 = 0)$ seeding resonance and the island chains at the top and bottom of Fig.2 are the $(f_1 = 1200Hz, n_1 = 1, f_2 = 50Hz, n_2 = \pm 1)$ sidebands of the $50Hz$ modulation. For $I_x = 3.4 \cdot 10^{-9} m$ the $(20, 0, -626)$ resonance sidebands become more dominant then the ones of the $(10, 0, -313)$ mode, and we see twenty resonance islands, rather than ten for the lower $50Hz$ sideband. Fig.2 illustrates the good agreement between the resonance positions calculated with the FFT mode amplitudes and the tracking data. For $I_z = 0$, the analytically calculated resonance positions from the left-hand side of Fig.2 agree nicely with the island positions in the right-hand side of Fig.2. With increasing ΔQ_{1200Hz}, the widths of the seeding sidebands increase, but they will never overlap with each other unless we introduce an additional modulation frequency. For example, for an additional tune modulation with $24Hz$ and $\Delta Q_{24Hz} = 8.0 \cdot 10^{-5}$ the seeding resonances overlap and result in a wide modulational layer. Because of the potential overlap of the seeding resonances, such an additional tune modulation with $24Hz$ is extremely dangerous. Even though a $24Hz$ modulation does not appear in the ripple spectrum of the power supplies for the proton ring in HERA, it might appear due to the vibration of the vacuum pumps [12] [16] or in the frequency spectrum of the ground motion. We will return to both possibilities later, when we compare the analytical estimates for the drift coefficients with the tracking data. Without any additional tune modulation, the seeding resonances do not lead to a drastic increase in the particle diffusion. Only in combination with an additional slow tune modulation or an explicitly stochastic signal, the seeding resonances of the fast tune modulation can cause a strong particle diffusion.

Because the low order sidebands of the $(7, 0, -219)$ resonance can not reach into the volume V_{beam} for the parameter values (5), we consider here only the $(10, 0, -313)$ resonance. However, for other parameter values, the sidebands of the $(7, 0, -219)$ resonance might also become important and have to be included in the diffusion analysis.

3.2 Slow Tune Modulation

In the case of a purely harmonic tune modulation, the emittance might only increase if we introduce an additional slow tune modulation. We consider the following range of slow modulation frequencies, as it dominates for example the frequency spectrum of the ground motion in the HERA tunnel[12]:

$$f_{slow} \in [0Hz, 10Hz]. \tag{22}$$

Depending on the number of slow modulation frequencies, their depths and values, the tune modulation can lead to three qualitatively different situations:

a) the tune modulation leads to a small stochastic layer around the separatrix of a nonlinear resonance,
b) the overlap of a large number of modulation sidebands leads to a homogeneous modulational layer,
c) the sideband overlap leads to a non-uniform modulational layer, which captures regions of stable motion.

In the following we will briefly discuss these three situations. For the sake of simplicity, we limit the following discussion to a purely horizontal driving Hamiltonian. Because $I_z \equiv 0$ is a solution to the equations of motion corresponding to (3), we can construct a two-dimensional surface of section for this special situation. Such a two-dimensional surface of section depicts clearly the resonance structure of the driving Hamiltonian and gives a nice illustration for the different cases. However, the restriction to a purely horizontal driving resonances is not a principal limitation, but serves only for a clear illustration of the various modulation effects.

a) If the slow tune modulation leads to a small stochastic layer around the separatrix of the seeding resonance, the particles inside the stochastic layer might spread in phase space due to the random nature of the motion. Chirikov called this diffusion mechanism the 'stochastic pump diffusion' [5], and we analyzed its significance for the particle motion in a storage ring in [3]. The analysis showed that even though the diffusion and drift coefficients can reach values of the same order of magnitude as the ones measured in the HERA-p storage ring, the stochastic pump diffusion is limited to a very small tune interval.

b) The overlap of a large number of slow modulation sidebands $(N >> 1)$ can lead to the formation of a uniform modulational layer and to a particle diffusion over relatively large tune intervals. A diffusion due to the random motion inside the modulational layer was described by [8]. Here, we extend the analysis in [8] to the motion of a particle in a storage ring, and look at its significance for a storage ring like HERA. In order to give a criterion for the formation of a uniform modulational layer it is convenient to introduce the overlap parameter s [5], defined as the ratio between the sum of the half-widths of two neighbouring sidebands and their relative spacing. If we expand (17) and (18) into a Taylor series around a stable fixed point, and neglect the derivatives of the $\tilde{A}_{l,0,k}$ mode with respect to the action I_x, we get for the sideband spacing

$$\Delta I_{spacing} = \frac{2\pi}{l \cdot L} \cdot \frac{\vec{n}_{fast} \cdot \vec{\Omega}_{fast} + \vec{n}_{slow} \cdot \vec{\Omega}_{slow}}{\partial^2 A_{0,0,0} / \partial I_x^2}, \tag{23}$$

and for the sideband width

$$\Delta I_{width} = \sqrt{\left|\frac{4 \cdot \tilde{A}_{l,m,k}}{\partial^2 A_{0,0,0}/\partial I_x^2}\right|}. \tag{24}$$

Using the FFT values for the mode amplitudes of the beam-beam kicks, we can calculate the sideband widths and their relative spacing in action space. For the parameter values (5) we have for example

$I_x = 4.8 \cdot 10^{-9} m;$	$I_z = 0.0m$
$A_{0,0,0} = 44.0 \cdot 10^{-16}$	$A_{10,0,-313} = 0.26 \cdot 10^{-16}$
$\frac{\partial^2 A_{0,0,0}}{\partial I_x^2} = -37.0$	$\frac{\partial^2 A_{10,0,-313}}{\partial I_x^2} = -1.28$

(25)

The critical value for s above which the sidebands overlap is $s = 2/\pi$, which is also called the 'two-thirds rule'[4]. If we apply this criterion to (17), look at only one resonance mode, and approximate the amplitude of the Besselfunctions for the slow modulation frequencies in $\tilde{A}_{l,0,k,\vec{n}_{fast},\vec{n}_{slow}}$ by their root-mean-square (rms) values, we get for the overlap condition

$$\frac{\pi^4 s^4}{16} = \frac{l^4 L^4 \tilde{A}^2_{l,m,k,\vec{n}_{fast}} \cdot \left(\frac{\partial^2 A_{0,0,0}}{\partial I_x^2}\right)^2}{\left[\left(\vec{n}_{slow} - \vec{n}'_{slow}\right) \cdot \vec{\Omega}_{slow}\right]^4} \times \prod_{p=1}^{N} \left(\frac{\Omega_p}{\pi l \Delta Q_p}\right) > 1, \tag{26}$$

where we have assumed the validity of (23) and (24). The overlap condition (26) indicates a resonance overlap for sufficiently small modulation frequencies, or for modulational frequencies which are sufficiently close to another. In the case of one slow modulation frequency, one expects the existence of a modulational layer once the modulation frequency is slower than the critical frequency

$$\Omega_{crit} = \left(\frac{l^3 L^4 \tilde{A}^2_{l,0,k,\vec{n}_{fast}} \cdot \left(\frac{\partial^2 A_{0,0,0}}{\partial I_x^2}\right)^2}{\pi \Delta Q_{slow}}\right)^{1/3}. \tag{27}$$

c) However, the limit $\Omega \to 0$ does not always lead to a uniform modulational layer. In the limit $\Omega_{slow} \to 0$ and constant modulation depth $\Delta Q_{slow,p}$, the chaotic region of the modulational layer merges into a single-resonance layer and leaves a stable region around the stable fixed points of the seeding resonance [17][4]. The stable region is bounded by KAM tori [18] and oscillates inside the modulational layer. Because the particles inside this stable region can not leave the KAM tori, the phenomenon is called 'trapping' [17][19]. In comparison with the modulational diffusion [8], the single-resonance trapping layer corresponds to a much weaker diffusion. (We will give an example for this slow diffusion process in a later section, when we compare the analytical estimates for the drift coefficients with tracking data.) For one slow modulation frequency, the condition for trapping can be expressed as [8]

$$l \cdot \tilde{A}_{l,m,k,\vec{n}_{fast}} \cdot \frac{\partial^2 A_{0,0,0}}{\partial I_x^2} > \frac{4\pi^2 \Delta Q_{slow} \Omega_{slow}}{L^2}, \tag{28}$$

where we have again assumed the validity of (23) and (24). For $\Omega_{slow} = 0$, the single-resonance trapping layer disappears all together, and only the stochastic layer of the un-modulated seeding resonance remains.

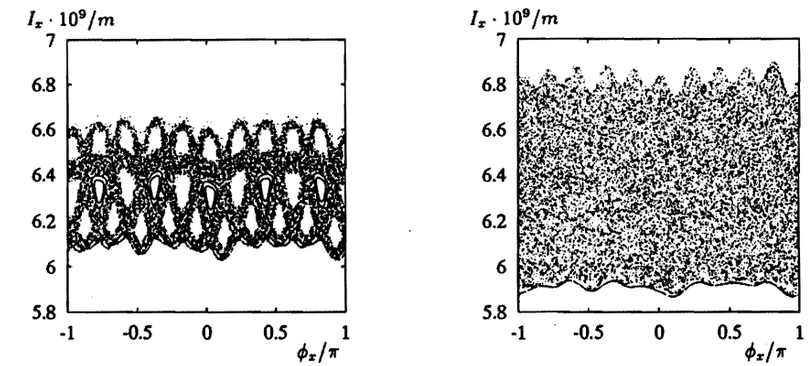

Figure 3: Resonance overlap for a tune modulation with one slow frequency.
Left: The stochastic layer around the ($f_1 = 1200Hz, n_1 = 1, f_2 = 50Hz, n_2 = -1$) seeding resonance of the $(10, 0, -313)$ mode for a slow modulation frequency of $3.3Hz$. One clearly recognizes the regions of regular motion inside the layer.
Right: The modulational layer for a slow modulation frequency of $0.6Hz$. In each case, the modulation depth is $\Delta Q_{slow} = 6.2 \cdot 10^{-6}$

At the end of this section we will briefly illustrate the resonance overlap and trapping with tracking data. We start with the overlap condition. Looking at the ($f_1 = 1200Hz, n_1 = 1, f_2 = 50Hz, n_2 = -1$) seeding resonances with modulation depths $\Delta Q_{1200Hz} = 1.25 \cdot 10^{-4}$ and $\Delta Q_{50Hz} = 4.38 \cdot 10^{-4}$, we get for the amplitude of the seeding resonance

$$\tilde{A}_{10,0,-313,1,-1} = J_1\left(\frac{10 \cdot \Delta Q_{1200Hz}}{\Omega_{1200Hz}}\right) \cdot J_1\left(\frac{10 \cdot \Delta Q_{50Hz}}{\Omega_{50Hz}}\right) \cdot A_{l,m,k} \approx 10^{-19}. \tag{29}$$

For an additional slow tune modulation with $\Delta Q_{slow} = 6.3 \cdot 10^{-5}$, we obtain a sideband overlap for modulation frequencies smaller then

$$2.0Hz \to (\Omega_{crit.} = 1/23000). \tag{30}$$

The rms value of the modulation depth has the same order of magnitude as the tune modulation due to the ground motion in the HERA tunnel ($\Delta_{rms} Q_x = O(10^{-5})$) [12]. Let us look at two different values for the slow modulation frequency:

$f_{slow,1} = 0.6Hz \to \Omega_{slow,1} = 1/76800$	$\Delta Q_{slow,1} = 6.2 \cdot 10^{-5}$
$f_{slow,2} = 3.3Hz \to \Omega_{slow,2} = 1/14400$	$\Delta Q_{slow,2} = 6.2 \cdot 10^{-5}.$

(31)

Neither of the frequencies fulfills the trapping condition (28). The left-hand side of Fig.3 shows the stochastic layer for the $3.3Hz$ modulation. As the modulation frequency is just above the critical frequency of the 'two-thirds rule', the sidebands do not fully overlap and the

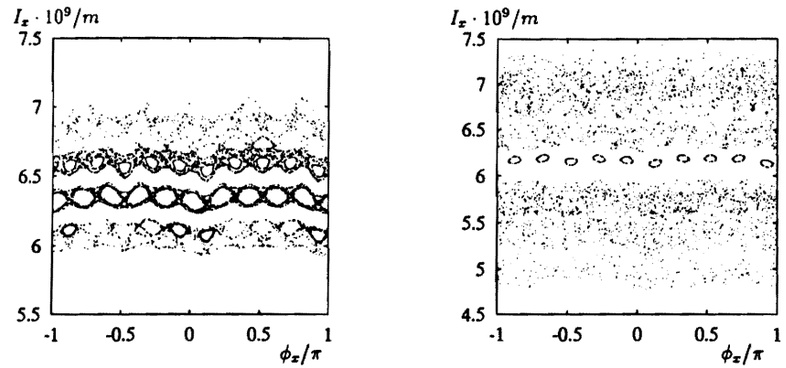

Figure 4: The combined effect of two slow modulation frequencies.
Left: The modulation sidebands of a slow $2.2Hz$ modulation around the $(f_1 = 1200Hz, n_1 = 1, f_2 = 50Hz, n_2 = -1)$ seeding resonance of the $(10, 0, -313)$ mode.
Right: The modulational layer for a simultaneous slow tune modulation with $2.2Hz$ and $3.3Hz$. In each case, the net rms modulation depth is $\Delta_{rms}Q_x = 3.1 \cdot 10^{-6}$

modulational layer still contains regions of regular motion. The right-hand side of Fig.3 shows the modulational layer for the $0.6Hz$ modulation. Here, the modulation frequency is clearly below the critical modulation frequency of the 'two-thirds rule', and we see a wide stochastic layer without any region of regular motion. In the following, we call such a stochastic layer a homogeneous modulational layer.

If we have more than one slow modulation frequency, the sidebands might form a homogeneous modulational layer even if each modulation frequency alone does not fulfill the overlap condition of the 'two-thirds rule'. This aspect is important for a tune modulation due to the ground motion, where we have a large number of modulation frequencies, and for the overlap of more than one fast seeding frequency. We will give one example for each case. The frequency spectrum of the ground motion in the HERA tunnel has a large number of modulation frequencies between $2Hz$ and $10Hz$ [12]. Even if each of these slow modulation frequencies alone does not lead to a homogeneous modulational layer, the simultaneous modulation with all frequencies might lead to a modulational layer. In order to illustrate this effect, we look at the two slow modulation frequencies

$$\boxed{f_{slow,2} = 3.3Hz \rightarrow \Omega_{slow,2} = 1/14400} \; \boxed{f_{slow,3} = 2.2Hz \rightarrow \Omega_{slow,1} = 1/21600.} \tag{32}$$

Each modulation frequency alone with a modulation depth $\Delta Q_p = 6.2 \cdot 10^{-5}$ is above the critical frequency of the 'two-thirds rule' (30), and the sidebands do not fully overlap. The left-hand side of Fig.3 shows the modulation sidebands of the $3.3Hz$ modulation in the horizontal surface of section and the left-hand side of Fig.4 shows the modulation sidebands of the $2.2Hz$ modulation. In each case, we used a fast tune modulation with $\Delta Q_{1200Hz} = 1.25 \cdot 10^{-4}$ and

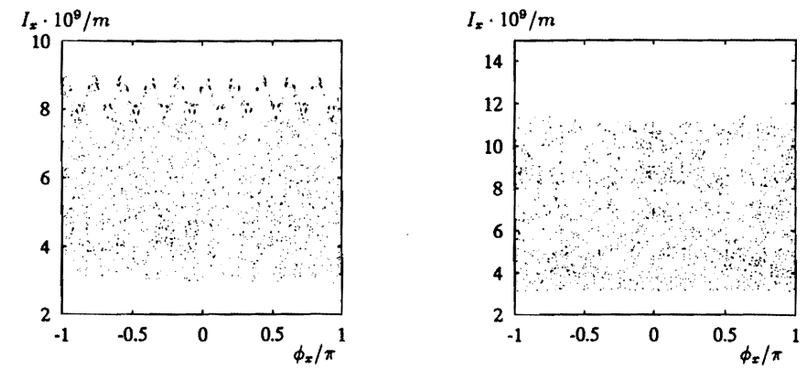

Figure 5: The effect of more than one fast modulation frequency with large amplitude.
Left: A simultaneous tune modulation with $1200Hz$ and $24Hz$. The sideband overlap leads to a homogeneous modulational layer.
Right: A simultaneous tune modulation with three fast frequencies $(f_{fast,1} = 1200Hz, f_{fast,2} = 50Hz, f_3 = 24Hz)$ leads to an even wider modulational layer.

$\Delta Q_{50Hz} = 4.38 \cdot 10^{-4}$, and in both cases we used a slow modulation depth of $\Delta Q_{slow} = 6.2 \cdot 10^{-5}$. One clearly recognizes the regions of stable motion embedded in the stochastic layers for both cases. For a simultaneous tune modulation with both frequencies and the same net rms modulation depth, the sidebands of the two frequencies overlap and form two homogeneous modulational layers which are separated by the $(f_1 = 1200Hz, n_1 = 1, f_2 = 50Hz, n_2 = -1)$ island chain. The resulting homogeneous modulational layers are depicted in the right-hand side of Fig.4. We will give another example for the sideband overlap of more than one modulation frequency. Even if we have no slow modulation frequency at all, the combined effect of one or two fast modulation frequencies together with an $24Hz$ modulation can lead to a homogeneous modulational layer, which extents over a large region of the phase space. If we increase for example the amplitude of the $1200Hz$ modulation to $\Delta Q_{1200Hz} = 2.5 \cdot 10^{-3}$ and introduce a third modulation frequency in the intermediate frequency regime

$$f_3 = 24Hz, \qquad \Delta Q_3 = 1.0 \cdot 10^{-4}, \tag{33}$$

the additional modulation sidebands overlap with the $(f_1 = 1200Hz, n_1 = 1, f_2 = 50Hz, n_2 = 0)$ and $(f_1 = 1200Hz, n_1 = 1, f_2 = 50Hz, n_2 = \pm 1)$ seeding resonances and result in an extremely wide modulational layer. Fig.5 shows the modulational layer in the horizontal surface of section. The left-hand side of Fig.5 shows the modulational layer caused by the $1200Hz$ and $24Hz$ modulation alone, and the right-hand side of Fig.5 shows the resulting wide modulational layer of a modulation with all three frequencies. The third modulation frequency (33) might be caused by the vibrations of the vacuum pumps [12][16] or by the ground motion in the HERA tunnel.

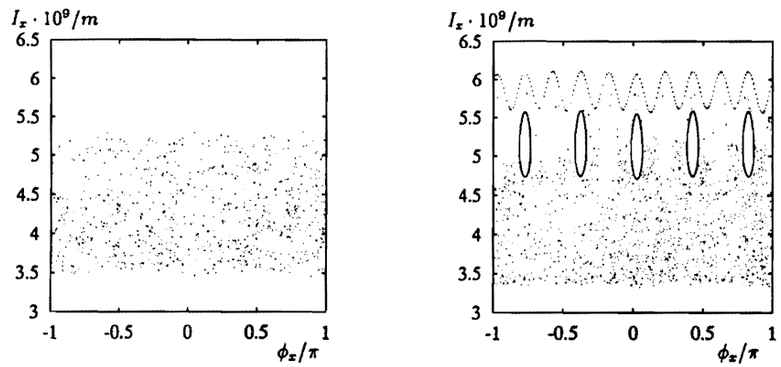

Figure 6: Particle trapping.
Left: The stochastic layer around the ($f_1 = 1200Hz, n_1 = 1$) seeding resonance for a slow tune modulation with $0.6Hz$ ($\Delta Q_{0.6Hz} = 6.26 \cdot 10^{-5}$) and $\Delta Q_{1200Hz} = 1.25 \cdot 10^{-4}$.
Right: The stochastic layer for a slow modulation frequency with $0.6Hz$ ($\Delta Q_{0.6Hz} = 6.26 \cdot 10^{-5}$) and $\Delta Q_{1200Hz} = 1.25 \cdot 10^{-3}$. One clearly recognizes the regions of regular motion inside the modulational layer.

Second, we illustrate the trapping phenomenon with tracking data. If we increase the modulation depth of the fast $1200Hz$ modulation, the $\tilde{A}_{l,0,k,\vec{n}_{fast}}$ mode amplitude also increases. For $\Delta Q_{1200Hz} = 1.25 \cdot 10^{-3}$, the mode amplitude

$$\tilde{A}_{10,0,-313,1,-1} = J_1\left(\frac{10 \cdot \Delta Q}{\Omega_{fast}}\right) \cdot A_{10,0,-313} \approx 6.3 \cdot 10^{-18}, \tag{34}$$

becomes large enough to fulfill the trapping condition (28) for an additional $0.6Hz$ modulation with $\Delta Q_{slow} = 6.26 \cdot 10^{-5}$. Fig.6 shows the corresponding surface of section in the horizontal phase space. The left-hand side of Fig.6 shows the surface of section for $\Delta Q_{1200Hz} = 1.25 \cdot 10^{-4}$, and the right-hand side for $\Delta Q_{1200Hz} = 1.25 \cdot 10^{-3}$. While we see a homogeneous modulational layer for $\Delta Q_{1200Hz} = 1.25 \cdot 10^{-4}$, one clearly recognizes the stable regions inside the modulational layer in the right-hand side of Fig.6. Over time, these stable regions oscillate between the top and the bottom of the modulational layer and reduce the particle diffusion. We will give an example for the reduction of the emittance growth due to the trapping phenomenon in a later section, where we compare our analytical estimates with tracking data.

At the end of this section, we want reemphasize, that all the above mentioned modulation frequencies arise naturally in a real storage ring. The rms modulation depths for the slow tune modulations has the same order of magnitudes as the ones caused by the ground motion in the HERA-p storage ring, and the fast modulation frequencies appear in the natural spectrum of the HERA-p power supplies.

Before we start our discussion of the diffusion mechanism, we will briefly discuss the particle motion on the coupling resonance and its effect on the resonance structure of our model Hamiltonian.

4 The Coupling Resonance

Because the proton distribution in HERA lies directly on the coupling resonance, we have to include the coupling resonance in our diffusion analysis. In this section we will look at the effect of the coupling resonance on the particle motion. The analysis consists of three parts. In a first step, we neglect the tune modulation and the $\tilde{A}_{l,m,k}$ modes and evaluate the particle motion on the unperturbed coupling resonance. In a second and third step, we re-introduce the tune modulation and the $\tilde{A}_{l,m,k}$ modes respectively.

The mode amplitudes of the $\tilde{A}_{l,m,k,\vec{n}_{fast}}$ seeding resonances are much smaller than the coupling mode amplitude and the zeroth order mode amplitude $A_{0,0,0}$. In a first approximation, we can therefore neglect the $\tilde{A}_{l,m,k,\vec{n}_{fast}}$ modes in (7) and look at the Hamilton function

$$H = \nu_x \cdot I_x + \nu_z \cdot I_z + A_{0,0,0}(I_x, I_z) + \tag{35}$$
$$\sum_{\vec{r}_{fast},\vec{r}_{slow}} \tilde{A}_{2,-2,2,\vec{r}_{fast},\vec{r}_{slow}} \cdot \cos\left(2\phi_x - 2\phi_z + \frac{2\pi}{L}\left(2 + \vec{r}_{fast} \cdot \vec{\Omega}_{fast} + \vec{r}_{slow} \cdot \vec{\Omega}_{slow}\right) s + \delta_{2,-2,2}\right).$$

Using the canonical transformation

$$F_2 = I_+ \cdot \frac{(\phi_x + \phi_z)}{2} + I_- \cdot \left[\frac{(\phi_x - \phi_z)}{2} + \frac{\pi \cdot s}{L}\right], \tag{36}$$

we change to the new variables

$$I_- = (I_x - I_z), \quad \phi_- = \frac{(\phi_x - \phi_z)}{2} + \frac{\pi \cdot s}{L} \tag{37}$$

$$I_+ = I_x + I_z, \quad \phi_+ = \frac{(\phi_x + \phi_z)}{2}, \tag{38}$$

and write the Hamilton function (35) as

$$\begin{aligned} H &= \frac{I_+}{2} \cdot (\nu_x + \nu_z) + \frac{I_-}{2} \cdot \left(\nu_x - \nu_z + \frac{\pi}{L}\right) + A_{0,0,0}(I_+, I_-) \\ &+ \sum_{\vec{r}_{fast},\vec{r}_{slow}} \tilde{A}_{2,-2,2,\vec{r}_{fast},\vec{r}_{slow}} \cdot \cos\left(4\phi_- + \frac{2\pi}{L}\left(\vec{r}_{fast} \cdot \vec{\Omega}_{fast} + \vec{r}_{slow} \cdot \vec{\Omega}_{slow}\right) s + \delta_{2,-2,2}\right). \end{aligned} \tag{39}$$

The new variable I_+ corresponds to the sum of the old actions and I_- to the difference of the horizontal and vertical actions. As the new Hamilton function does not depend on the angle ϕ_+, the total action is a constant of the motion and the equations of motion for the remaining degree of freedom reduce to the coupled differential equations:

$$\dot{I}_- = 4 \cdot \sum_{\vec{r}_{fast},\vec{r}_{slow}} \tilde{A}_{2,-2,2,\vec{r}_{fast},\vec{r}_{slow}} \cdot \sin\left(4\phi_- + \left[\vec{r}_{fast} \cdot \vec{\Omega}_{fast} + \vec{r}_{slow} \cdot \vec{\Omega}_{slow}\right] s + \delta_{2,-2,2}\right) \tag{40}$$

$$\begin{aligned} \dot{\phi}_- &= \frac{1}{2} \cdot \left(\nu_x - \nu_z + \frac{\pi}{L}\right) + \frac{\partial A_{0,0,0}}{\partial I_-}(I_+, I_-) \\ &+ \sum_{\vec{r}_{fast},\vec{r}_{slow}} \frac{\partial \tilde{A}_{2,-2,2,\vec{r}_{fast},\vec{r}_{slow}}}{\partial I_-} \cdot \cos\left(4\phi_- + \left[\vec{r}_{fast} \cdot \vec{\Omega}_{fast} + \vec{r}_{slow} \cdot \vec{\Omega}_{slow}\right] s + \delta_{2,-2,2}\right). \end{aligned}$$

For the moment, we neglect the tune modulation in (40). In the vicinity of the stable fixed points $I_{-,res+}$ and $\phi_{-,res+}$, the equations of motion reduce to the differential equations of a harmonic oscillator with frequency

$$\omega_{lib.} = 2 \cdot \sqrt{-\tilde{A}_{2,-2,2} \cdot \left(\frac{\partial^2 A_{0,0,0}}{\partial I_-^2} + \frac{\partial^2 A_{2,-2,2}}{\partial I_-^2} \cdot \cos\left(\phi_{-,res+} + \delta_{2,-2,2}\right) \right)}, \tag{41}$$

with the linear solutions

$$I_{-,0}(s) = I_{-,res+} - \Delta I_{-,lib.} \cdot \cos\left(\omega_{lib.} \cdot s + \theta_0\right) \tag{42}$$

$$\phi_{-,0}(s) = \phi_{-,res+} + \frac{\omega}{\tilde{A}_{2,-2,2}} \Delta I_- \cdot \sin\left(\omega_{lib.} \cdot s + \theta_0\right). \tag{43}$$

With increasing $\Delta I = \mid I_- - I_{-,res+} \mid$, the frequency decreases and approaches zero, as I_- reaches the separatrix of the coupling resonance. We call the motion inside the separatrix libration and the motion outside the separatrix rotation [4]. For the parameter values (5) and for $(I_x = I_z)$ we get for example

$I_x = 4.0 \cdot 10^{-9} m = I_z$		
$A_{0,0,0} = 58.4 \cdot 10^{-16}$	$A_{2,-2,2} = -4.41 \cdot 10^{-16}$	$A_{10,0,-313} = 0.0345 \cdot 10^{-16}$
$\frac{\partial^2 A_{0,0,0}}{\partial I_x^2} = -30.0$	$\frac{\partial^2 A_{0,0,0}}{\partial I_x I_z} = -19.0$	$\frac{\partial^2 A_{0,0,0}}{\partial I_z^2} = -30.0$
$\frac{\partial^2 A_{2,-2,2}}{\partial I_x^2} = 1.68$	$\frac{\partial^2 A_{2,-2,2}}{\partial I_x I_z} = -4.22$	$\frac{\partial^2 A_{2,-2,2}}{\partial I_z^2} = 1.35$
$\frac{\partial^2 A_{10,0,-313}}{\partial I_x^2} = -0.29$	$\frac{\partial^2 A_{10,0,-313}}{\partial I_x I_z} = -0.319$	$\frac{\partial^2 A_{10,0,-313}}{\partial I_z^2} = 0.06$
$I_x = 2.4 \cdot 10^{-9} m = I_z$		
$A_{0,0,0} = 48.7 \cdot 10^{-16}$	$A_{2,-2,2} = -3.8 \cdot 10^{-16}$	$A_{10,0,-313} = 0.01 \cdot 10^{-16}$
$\frac{\partial^2 A_{0,0,0}}{\partial I_x^2} = -81.3$	$\frac{\partial^2 A_{0,0,0}}{\partial I_x I_z} = -50.5$	$\frac{\partial^2 A_{0,0,0}}{\partial I_z^2} = -82.3$
$\frac{\partial^2 A_{2,-2,2}}{\partial I_x^2} = 6.85$	$\frac{\partial^2 A_{2,-2,2}}{\partial I_x I_z} = -10.2$	$\frac{\partial^2 A_{2,-2,2}}{\partial I_z^2} = 5.51$
$\frac{\partial^2 A_{10,0,-313}}{\partial I_x^2} = -0.295$	$\frac{\partial^2 A_{10,0,-313}}{\partial I_x I_z} = -0.34$	$\frac{\partial^2 A_{10,0,-313}}{\partial I_z^2} = 0.05$

(44)

and thus, for the free island oscillation frequency of the libration

$I_x = 4.0 \cdot 10^{-9} m = I_z$	
Theory	Tracking
$\omega_{libration} \approx 2\pi/(L \cdot 4100)$	$\omega_{libration} \approx 2\pi/(L \cdot 3900)$
$I_x = 2.4 \cdot 10^{-9} m = I_z$	
Theory	Tracking
$\omega_{libration} \approx 2\pi/(L \cdot 2600)$	$\omega_{libration} \approx 2\pi/(L \cdot 2500)$

(45)

The tracking data was obtained by a successive application of (13) to the particle coordinates. The data agrees nicely with the analytically calculated values and illustrates the validity of our approximations. Outside the separatrix, the ϕ_- phase no longer oscillates, but increases with every turn. However, I_- might still oscillate with a small amplitude if the particle motion is close to the separatrix. The frequency for the I_- oscillation during rotation is given by the difference in the horizontal and vertical tunes

$$\omega_{rot.} = \frac{4\pi}{L} \cdot (Q_x - Q_z + 1), \tag{46}$$

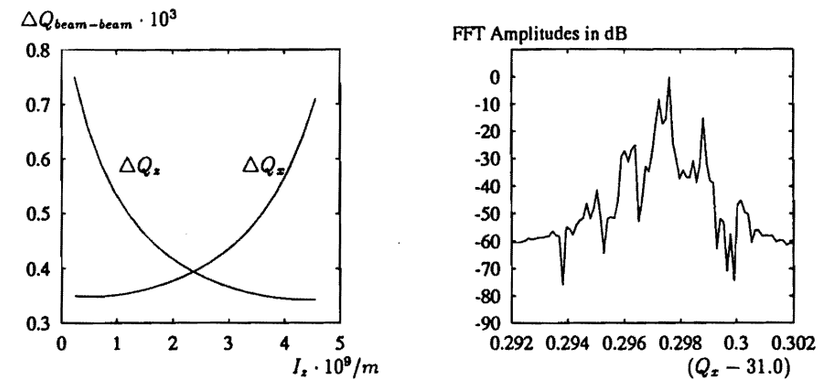

Figure 7:
Left: The horizontal and vertical detuning ΔQ due to the I_- oscillation and the beam-beam detuning for $(I_x + I_z) = 4.8 \cdot 10^{-9} m$.
Right: The horizontal Fourier spectrum for the particle motion on the coupling resonance with tune modulation.

and we can write the linear solutions of the action-angle variables as

$$I_{-,0} = I_{-,rot.} + \Delta I_{-,rot.} \cdot \cos\left(\omega \cdot s + \theta_0\right) \tag{47}$$

$$\phi_{-,0} = \phi_{res,rot.} + \frac{\omega_{rot.}}{4} \cdot s. \tag{48}$$

In other words: without any tune modulation the total action I_+ is a constant of motion and the energy of the transversal motion oscillates between the horizontal and vertical plane with a frequency ω.

The energy oscillation has a dramatic effect on the horizontal and vertical tunes. Because of the change in I_x and I_z during the I_- oscillation, the horizontal and vertical Q-values (Q_x and Q_z) also oscillate due to the beam-beam detuning. For example, for $(< I_x >= 2.4 \cdot 10^{-9} m =< I_z >)$, the horizontal and vertical detuning ΔQ_x varies between $(\Delta Q_x = 0.35 \cdot 10^{-3})$ and $(\Delta Q_x = 0.7 \cdot 10^{-3})$. Thus, the I_- oscillation leads to a tune modulation in the intermediate frequency range between the slow and the fast modulation frequencies. In comparison with the slow tune modulation due to the ground motion (31), the tune modulation due to the coupling resonance is very strong. The left-hand side of Fig.7 shows the horizontal and vertical detuning as a function of the vertical action I_z with the constraint $(I_x + I_z) = 4.8 \cdot 10^{-9} m$. The right-hand side of Fig.7 shows the horizontal FFT spectrum of one particle on the coupling resonance with a fast tune modulation of $1200 Hz$ and $50 Hz$. (The spectrum shows the fractional part of the horizontal Q_x-value.) One clearly recognizes the first two upper and lower $50 Hz$ sidebands around the horizontal Q-value ($Q_x = 31.2978$). Each sideband has a spacing of $\Delta Q_x(50 Hz) \approx 1.25 \cdot 10^{-3}$ and splits again into sidebands of a $16.5 Hz$ modulation due to the motion on the coupling resonance. The spacing of these additional sidebands is

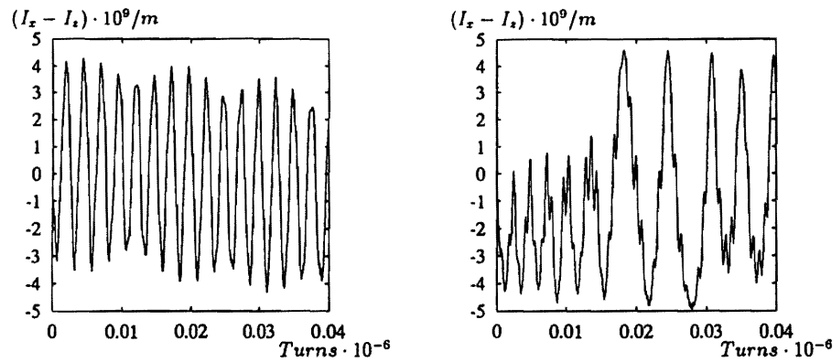

Figure 8:
Left: The energy oscillation on the coupling resonance with tune modulation and close to the stable fixed point ($\phi_-(s=0) \approx \pi/2$).
Right: The energy oscillation on the coupling resonance with tune modulation and within the stochastic layer of the coupling resonance ($\phi_-(s=0) \approx 0.0$).
For both pictures, we used ($Q_x - Q_z + 1 = 0.0$).

$\Delta Q_x(16Hz) \approx 1/2900$, which corresponds nicely to the free island oscillation frequency (45).

In a second step, we introduce again a horizontal tune modulation and look at its effect on the resonance structure of the coupling resonance. For the fast $1200Hz$ tune modulation, the sidebands of the coupling resonance can not overlap, and the motion on the coupling resonance remains regular. For the $50Hz$ seeding frequency, the sidebands of the coupling resonance might overlap, but because the argument of the Besselfunctions in (10) is small, only the first two sidebands might overlap, and the overlap can lead only to a small stochastic layer around the separatrix of the coupling resonance. For the slow tune modulation, the trapping condition is fulfilled, and the tune modulation leads again only to a small stochastic layer around the separatrix of the coupling resonance. Hence, in the direct neighbourhood of the stable fixed points of the coupling resonance, the particle motion remains regular, and the tune modulation can not lead to a homogeneous modulational layer. Only if we introduce a tune modulation in the intermediate frequency range ($f \in [10Hz, 50Hz]$), as for example a tune modulation of $24Hz$ due to the vibration of the vacuum pumps, can the modulation sidebands of the coupling resonance overlap in such a way as to lead to a homogeneous modulational layer.

The stochastic layer around the separatrix of the coupling resonance has two important effects on the particle motion. Inside the stochastic layer, the oscillation period of the I_- motion varies between an upper and lower bound, and the ϕ_- phase experiences a 'stochastic' variation during each half period of the I_- oscillation [5][4].

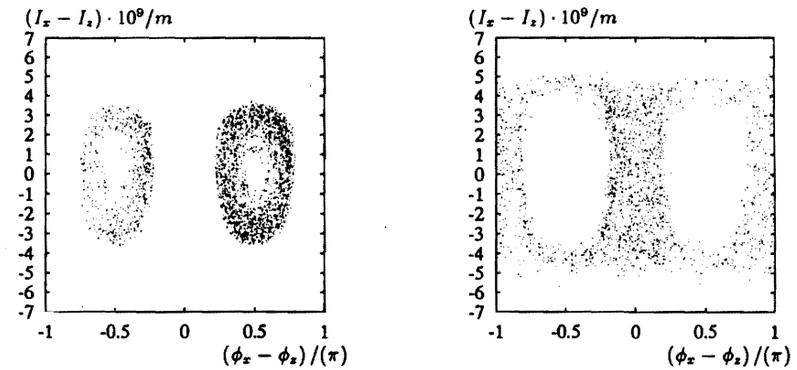

Figure 9:
Left: The stroboscobic phase space projection for the regular libration in the vicinity of the stable fixed points ($\phi_-(s=0) \approx \pi/2$).
Right: The phase space projection for the motion within the stochastic layer of the coupling resonance ($\phi_-(s=0) \approx 0.0$).
For both pictures, we used ($Q_x - Q_z + 1 = 0.0$).

We analyzed the stochastic pump diffusion due to the stochastic character of the motion inside the stochastic layer in [3] and will neglect the effect in the following. The right-hand side of Fig.8 shows $(I_x - I_z)$ versus the number of turns for a particle inside the stochastic layer of the coupling resonance. One clearly recognizes the random changes in the oscillation frequency of the $(I_x - I_z)$ motion due to the phase variation during each half period. If the particle is not inside the stochastic layer, one can neglect the influence of the tune modulation on the particle motion. For the libration inside the regular region of the coupling resonance, we can approximate the oscillation frequency by the linear solution (41), and for the regular rotation, we can use (46). The left-hand side of Fig.8 shows the $(I_x - I_z)$ oscillation near the stable fixed points of the coupling resonance. One clearly recognizes the regular character of the action oscillations. The existence of a criterion which states whether the particle motion is inside the stochastic layer or inside the regular part of the phase space would be desirable. Unfortunately, the mode amplitude of the coupling resonance is of the same order of magnitude as the detuning term $A_{0,0,0}$ and has a complicated dependence on the actions [3]. It is therefore not possible to calculate the resonance half width and the stochastic layer width with the help of the standard pendulum approximation [5][4]. Instead, we have to analyse each case individually with the help of numerical tracking. To this end, we look at the stroboscobic phase space projection of the particle motion. The left-hand side of Fig.9 shows the projection for the regular motion in the neighbourhood of the stable fixed points and the right-hand side shows the projection for the motion within the stochastic layer. One clearly recognizes the separatrix structure in the right-hand side of Fig.9.

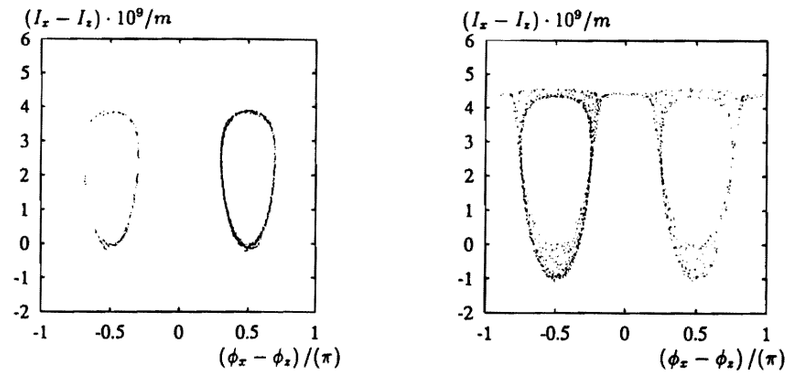

Figure 10:
Left: The stroboscobic phase space projection for $(Q_x - Q_z + 1 = 2.0 \cdot 10^{-4})$.
Right: The stroboscobic phase space projection for $(Q_x - Q_z + 1 = 2.8 \cdot 10^{-4})$.
For both pictures, we used the initial conditions $(I_-(s=0) = 0.0, \phi_-(s=0) = \pi/2)$.

Another interesting quantity is the resonance width in the Q-space. We will need this quantity in the next section, when we discuss the Q-dependence of the drift coefficients and compare the analytical estimates with tracking data. For $I_x \approx I_z$ and $(Q_x - Q_z + 1 = 0)$, the particles are right on the $(2, -2, 2)$ coupling resonance. If we keep the Q_x-value constant and decrease Q_z, the particles will leave the coupling resonance for $(Q_x - Q_z + 1 > \Delta Q_{res})$. ΔQ_{res} represents the width of the coupling resonance in the transverse Q-space. The left-hand side of Fig.10 shows the stroboscobic phase space projection for $(Q_x - Q_z + 1 < \Delta Q_{res})$ and the right-hand side of Fig.10 the projection for $(Q_x - Q_z + 1 = \Delta Q_{res})$. For both pictures, we used the parameter values (5) and the initial conditions $(I_x(s=0) = 2.2 \cdot 10^{-9} m = I_z(s=0)$, $\phi_-(s=0) = \pi/2)$. The tracking data from Fig.10 yields for the resonance width

$$\Delta Q_{res} = 2.8 \cdot 10^{-4}. \tag{49}$$

For $(Q_x - Q_z + 1 > \Delta Q_{res})$, the motion changes from libration to rotation and we have to use (47) and (48) instead of the linear solutions (42) and (43).

In a last step, we reconsider the $(10, 0, -313)$ seeding resonance. Because I_x and I_z oscillate on the coupling resonance, we have to look at the postion and width of the modulational layer in the whole horizontal action space. We can easily generalize equations (18), (23), and (24) for the case of non-vanishing I_z. The left-hand side of Fig.11 shows the resulting positions of the $1200Hz$ and $50Hz$ sidebands in the transverse action space for the horizontal $(10, 0, -313)$ sum resonance. The abscissa corresponds to the horizontal- and the ordinata to the vertical action. The solid line with dots shows the $(f_1 = 1200Hz, n_1 = 1, f_2 = 50Hz, n_2 = 0)$, seeding resonance and the two lines without dots show the upper and lower $(f_1 = 1200Hz, n_1 = 1, f_2 = 50Hz, n_2 = \pm 1)$ sidebands. The right-hand side of Fig.11 shows the resonance width of the

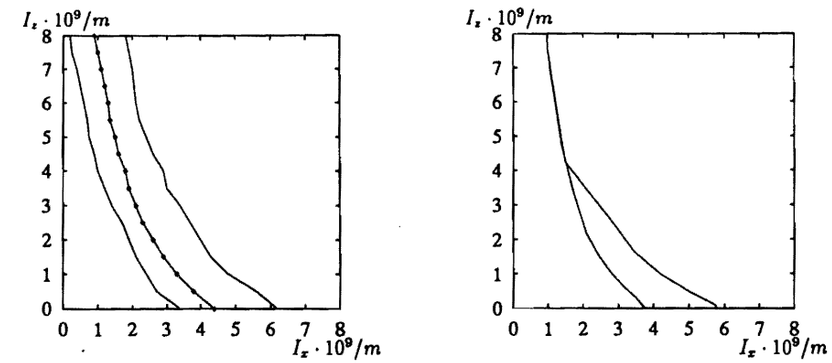

Figure 11:
Left: The position of the $(10, 0, -313)$ resonance sidebands in the horizontal action space for $Q_x = 31.2971$ and $Q_z = 32.2971$. The line with dots shows the positions of the $(f_1 = 1200Hz, n_1 = 1, f_2 = 50Hz, n_2 = 0)$ seeding resonance, and the two solid lines the position of the $(f_1 = 1200Hz, n_1 = 1, f_2 = 50Hz, n_2 = \pm 1)$ seeding resonances.
Right: The modulational layer around the $(f_1 = 1200Hz, n_1 = 1, f_2 = 50Hz, n_2 = 0)$ seeding resonance.

modulational layer around the $1200Hz$ seeding resonance with $(\Delta Q_{1200Hz} = 3.2 \cdot 10^{-4})$ for a slow tune modulation with $0.6Hz$ and $\Delta Q_{0.6Hz} = 6.25 \cdot 10^{-5}$, and for the case of rotational motion on the coupling resonance. (For the libration motion inside the regions of regular motion around the stable fixed points of the coupling resonance, the trapping condition (28) is fulfilled and the slow tune modulation does not lead to a homogeneous modulational layer.) During the I_x and I_z oscillation, the particles leave the modulational layer periodically. For $I_x > I_z$, the particles are inside the layer, and for $I_x < I_z$, the particles are outside the layer. Hence, for large oscillation amplitudes, the particles experience the random motion inside the modulational layer only during every second half period of the I_x/I_z oscillation. If we consider again all 10th order modes, we get a similar resonance pattern for all sum resonances, and the particles are always on one of the 10th order resonances.

We are now ready to analyze the particle diffusion and to calculate estimates of the drift coefficients and the emittance growth. In the next sections, we introduce the diffusion mechanism and compare the resulting analytical estimates with tracking data.

5 Particle Diffusion

In this section we will summarize the main aspects of the diffusion mechanism. A detailed description of the diffusion mechanism can be found in [8] [4] [20][21]. However, there are three important differences between the particle dynamics in our model structure and the assumptions made in [8] [4] [20] and [21]. In [8] [4], the authors assume a perturbed non-linear system with a coupling that is small compared to the driving resonance, and look only at one modulation frequency. In our model structure, we are dealing with a perturbed linear system and a coupling that is large compared to the driving resonance. In [20] [21], the authors look at a two-dimensional system in the single resonance approximation, and look again only at one modulation frequency. We look at a tune modulation with more than one frequency and consider the interaction of more than one beam-beam resonances in a four-dimensional, time dependent Hamilton system. Therefore, we have to modify the diffusion analysis before we can apply it to our problem.

The time evolution of the actions I_x and I_z is determined by Hamilton's equations

$$\frac{dI_y}{ds} = -\frac{\partial H}{\partial \phi_y}, \quad y = x, z. \tag{50}$$

We define the diffusion coefficient

$$D(I_x, I_z) = \frac{< \Delta I^2 >_\phi}{2T}, \tag{51}$$

with

$$\Delta I = -\int_{-T}^{T} \frac{\partial H}{\partial \phi}. \tag{52}$$

At this point we should recall that the horizontal and vertical actions do not stay constant inside the modulational layer, and that the change of the actions leads to a non-oscillating variation of the horizontal and vertical tunes. Thus, we have to average the diffusion coefficient (51) over the non-oscillating parts of the tune values inside the modulational layer. To this end, we define the tunes as

$$\nu_x(I_x, I_z) = \frac{2\pi}{L} Q_x + \frac{\partial A_{0,0,0}}{\partial I_x}(I_x, I_z), \tag{53}$$

$$\nu_z(I_x, I_z) = \frac{2\pi}{L} Q_z + \frac{\partial A_{0,0,0}}{\partial I_z}(I_x, I_z). \tag{54}$$

The diffusion coefficient (51) becomes now

$$D(I_x, I_z) = \frac{1}{8 \cdot \Delta\nu_x \cdot \Delta\nu_z \cdot T} \cdot \left\langle \int_{\Delta\nu_x}^{\Delta\nu_x} d\nu_x \int_{\Delta\nu_z}^{\Delta\nu_z} d\nu_z \int_{-T}^{T} \frac{\partial H}{\partial \phi}(s')ds' \times \int_{-T}^{T} \frac{\partial H}{\partial \phi}(s'')ds'' \right\rangle_\phi . \tag{55}$$

In order to evaluate the integrals in (55), we need an explicit expression for the phase variables $\phi_x(s)$ and $\phi_z(s)$. In order to solve the equations of motion corresponding to the action-angle variables, we introduce a small parameter ε and use perturbation theory. The analysis in [3]

showed, that for $(l+m) \geq 7$ and the parameter values (5), the mode amplitudes $A_{l,m,k}$ are small compared to the detuning term $A_{0,0,0}$ and the coupling mode $A_{2,-2,2}$. To emphasize this aspect, we write

$$\tilde{A}_{l,m,k,\vec{n}_{slow}} = \varepsilon \cdot \bar{A}_{l,m,k,\vec{n}_{slow}},$$

and decompose the action-angle variables into zeroth and first order parts

$$I(s) = I_0(s) + \varepsilon I_1(s); \qquad \phi(s) = \phi_0(s) + \varepsilon \phi_1(s). \tag{56}$$

In order to compare the analytical results for the particle diffusion with numerical data, we also need the corresponding drift coefficients. For Hamiltonian systems, the drift coefficient

$$B(I_x, I_z) = \frac{< \Delta I >_\phi}{2T}$$

can be calculated using the partial derivative of the diffusion coefficient with respect to the diffusing action variable [4]:

$$B(I_x, I_z) = \frac{1}{2} \cdot \frac{\partial D}{\partial I}(I_x, I_z). \tag{57}$$

We are now ready to calculate the drift and diffusion coefficients of our model structure. Because of the coupling near the $A_{2,-2,2}$ mode, the tracking data yields only drift coefficients for the total action $(I_x + I_z)$. Therefore, we use the coordinates (38)

$$I_- = (I_x - I_z), \quad \phi_- = \frac{(\phi_x - \phi_z)}{2} + \frac{\pi}{L}s \tag{58}$$

$$I_+ = I_x + I_z, \quad \phi_+ = \frac{(\phi_x + \phi_z)}{2}, \tag{59}$$

and refer in the following always to the drift and diffusion coefficients of the total action (I_+). For the discussion of the drift and diffusion coefficients, we distinguish four different situations:

a) the particles are away from the coupling resonance,
b) the particles perform a rotational motion near the coupling resonance,
c) the particles are on the coupling resonance and perform a libration inside the regular region of the coupling resonance,
d) the particles are subject to an explicitly stochastic tune variation.

a) If the particles are away from the coupling resonance, we can neglect the coupling mode in our Hamilton system and get

$$H = \nu_x \cdot I_x + \nu_z \cdot I_z + A_{0,0,0}(I_x, I_z) + \varepsilon \cdot \sum_{l,m,k,\vec{n}_{slow}} \tilde{A}_{l,m,k,\vec{n}_{fast},\vec{n}_{slow}}(I_x, I_z) \cdot \cos\left(l\phi_x + m\phi_z + \frac{2\pi}{L}\left(k + \vec{n}_{fast} \cdot \vec{\Omega}_{fast} + \vec{n}_{slow} \cdot \vec{\Omega}_{slow}\right) s + \delta_{l,k}\right), \tag{60}$$

with

$$\dot{I}_+ = \varepsilon \cdot \sum_{l,m,k,\vec{n}_{slow}} (l+m) \cdot \bar{A}_{l,m,k,\vec{n}_{fast},\vec{n}_{slow}}(I_x, I_z) \times \sin\left(l\phi_x + m\phi_z + \frac{2\pi}{L}\left(k + \vec{n}_{fast} \cdot \vec{\Omega}_{fast} + \vec{n}_{slow} \cdot \vec{\Omega}_{slow}\right) s + \delta_{l,k}\right). \tag{61}$$

For the zeroth-order solutions of the angle variables, we get

$$\phi_{x,0}(s) = \nu_x \cdot s + \theta_{x,0}, \qquad \phi_{z,0}(s) = \nu_z \cdot s + \theta_{z,0}. \tag{62}$$

The horizontal and vertical action variables vary inside the modulational layer of the seeding resonance. However, assuming that the $A_{l,m,k}$ mode amplitudes do not vary considerably inside the modulational layer, we can neglect the variations of the action variables and replace $A_{l,m,k}(I_x, I_z)$ by their average values inside the modulational layer. With these approximations and with the assumption [8]

$$T \cdot \Delta\nu_x \gg 2\pi, \tag{63}$$

we can solve the s'' integral in (55) and get for the diffusion coefficient

$$D(I_x, I_z) = \sum_{l,m,k} \frac{(l+m)^2\pi}{2l\Delta\nu_x} \cdot \left[\prod_{p=1}^{N} J_{n_{fast,p}}\left(\frac{l\Delta Q_{x,fast}}{\Omega_{fast,p}}\right)\right]^2 \cdot A^2_{l,m,k} \times \tag{64}$$
$$\sum_{[\vec{n}_{slow}-\vec{n}'_{slow}]\cdot\vec{\Omega}_{slow}=0} \left\{\left[\prod_{p=1}^{N} J_{n_{slow,p}}\left(\frac{l\cdot\Delta Q_{slow,p}}{\Omega_{slow,p}}\right)\right] \cdot \left[\prod_{p=1}^{N} J_{n'_{slow,p}}\left(\frac{l\cdot\Delta Q_{slow,p}}{\Omega_{slow,p}}\right)\right]\right\},$$

where $\Delta\nu_x$ is given by the maximum value of $\vec{n}_{slow}\cdot\vec{\Omega}_{slow}$ compatible with the overlap condition (26)

$$\Delta\nu_x = \frac{2\pi}{lL} \cdot \max_{overlap} \left(\vec{n}_{slow} \cdot \vec{\Omega}_{slow}\right), \tag{65}$$

and where the sums goes over all overlaping modulation sidebands with

$$\left(\frac{m}{l}\nu_z + \frac{2\pi}{lL} \cdot \left[\vec{n}_{fast} \cdot \vec{\Omega}_{fast} + (\vec{n}_{slow} - \vec{n}'_{slow}) \cdot \vec{\Omega}_{slow} + k\right]\right) \in [\nu_x - \Delta\nu_x,\ \nu_x + \Delta\nu_x]. \tag{66}$$

The corresponding drift coefficient of the total action $(I_x + I_z)$ becomes

$$B(I_x, I_z) = \sum_{l,m,k} \frac{(l+m)^2\pi}{2l\Delta\nu_x} \cdot \left[\prod_{p=1}^{N} J_{n_{fast,p}}\left(\frac{l\Delta Q_{fast,p}}{\Omega_{fast,p}}\right)\right]^2 \cdot A_{l,m,k} \cdot \left[\frac{\partial A_{l,m,k}}{\partial I_x} + \frac{\partial A_{l,m,k}}{\partial I_z}\right] \times \tag{67}$$
$$\sum_{\vec{n}_{slow},\vec{n}'_{slow}} \left\{\left[\prod_{p=1}^{N} J_{n_{slow,p}}\left(\frac{l\cdot\Delta Q_{slow,p}}{\Omega_{slow,p}}\right)\right] \cdot \left[\prod_{p=1}^{N} J_{n'_{slow,p}}\left(\frac{l\cdot\Delta Q_{slow,p}}{\Omega_{slow,p}}\right)\right]\right\}.$$

If the slow modulation frequencies have no common denominator

$$(\vec{n}_{slow} - \vec{n}'_{slow}) \cdot \vec{\Omega}_{slow} = 0 \rightarrow (\vec{n}_{slow} - \vec{n}'_{slow}) = 0, \tag{68}$$

the sum over the Bessel functions can be approximated by one [22], and we get

$$B(I_x, I_z) = \sum_{l,m,k} \frac{(l+m)^2\pi}{2l\Delta\nu_x} \cdot \left[\prod_{p=1}^{N} J_{n_{fast,p}}\left(\frac{l\Delta Q_{fast,p}}{\Omega_{fast,p}}\right)\right]^2 \cdot A_{l,m,k} \cdot \left[\frac{\partial A_{l,m,k}}{\partial I_x} + \frac{\partial A_{l,m,k}}{\partial I_z}\right]. \tag{69}$$

In the case of one slow modulation frequency, we can easily calculate the tune width $\Delta\nu_x$. Because the Bessel functions of the slow tune modulation have only significant values for $(n_p < l\Delta Q_{slow}/\Omega_{slow})$, the number of modulation sidebands inside the layer is approximately

$$N = 2 \cdot \frac{l\Delta Q_{slow}}{\Omega_{slow}}, \tag{70}$$

and we get for $\Delta\nu_x$

$$\Delta\nu_x = \frac{2\pi}{lL} \cdot \frac{l \cdot \Delta Q_{slow}}{\Omega_{slow}} \cdot \Omega_{slow}. \tag{71}$$

In this case, the diffusion coefficient reduces to the simple form

$$B(I_x, I_z) = \sum_{l,m,k} \frac{(l+m)^2 L}{4l\Delta Q_{slow}} \cdot \left[\prod_{p=1}^{N} J_{n_{fast,p}}\left(\frac{l\Delta Q_{fast,p}}{\Omega_{fast,p}}\right)\right]^2 \cdot A_{l,m,k} \cdot \left[\frac{\partial A_{l,m,k}}{\partial I_x} + \frac{\partial A_{l,m,k}}{\partial I_z}\right], \tag{72}$$

which agrees with the results in [20] and [21].

It is interesting to note that in the case of a rotational motion away from the coupling resonance, the drift and diffusion coefficients are proportional to the inverse of the slow modulation strengths. If the particles are not inside the modulational layer, or if the width of the modulational layer becomes too small for the approximation (63) to be valid, the drift and diffusion coefficients vanish.

b) If the particles perform a rotational motion near the coupling resonance, we can not neglect the coupling mode in our Hamilton function. We now have

$$H = \nu_x \cdot I_x + \nu_z \cdot I_z + A_{0,0,0}(I_x, I_z) + \tag{73}$$
$$\sum_{\vec{r}_{slow}} \tilde{A}_{2,-2,2,\vec{r}_{fast},\vec{r}_{slow}}(I_x, I_z) \cdot \cos\left(2\phi_x - 2\phi_z + \frac{2\pi}{L}\left(k + \vec{r}_{fast} \cdot \vec{\Omega}_{fast} + \vec{r}_{slow} \cdot \vec{\Omega}_{slow}\right) s + \delta_{2,2}\right) +$$
$$\varepsilon \sum_{l,m,k,\vec{n}_{slow}} \tilde{A}_{l,m,k,\vec{n}_{fast},\vec{n}_{slow}}(I_x, I_z) \cdot \cos\left(l\phi_x + m\phi_z + \frac{2\pi}{L}\left(k + \vec{n}_{fast} \cdot \vec{\Omega}_{fast} + \vec{n}_{slow} \cdot \vec{\Omega}_{slow}\right) s + \delta_{l,k}\right).$$

Because of the oscillations of the horizontal and vertical actions near the coupling resonance, the mode amplitudes $A_{l,m,k}$, their derivatives, and the beam-beam detuning term oscillate with the frequency ω_{rot} (46). The left-hand side of Fig.12 shows an example for one period of the horizontal and vertical action oscillations for the rotational motion, and the the right-hand side of Fig.12 shows the resulting changes in the mode amplitude $A_{10,0,-313}$ and its derivatives with respect to the horizontal and vertical actions. In both pictures, the total action is $I_+ = 4.4 \cdot 10^{-9} m$.

Replacing the mode amplitudes, their derivatives, and the beam-beam detuning by their Fourier expansions

$$A_{l,m,k} = \frac{a_{(l,m,k),0}}{2} + \sum_{q=1}^{\infty}\left[a_{(l,m,k),q} \cdot \cos\left(\frac{2\pi}{L} q\Omega_{coup.} s\right) + b_{(l,m,k),q} \cdot \sin\left(\frac{2\pi}{L} q\Omega_{coup.} s\right)\right], \tag{74}$$

$$\frac{\partial A_{l,m,k}}{\partial I_x} = \frac{c_{(l,m,k),0}}{2} + \sum_{q=1}^{\infty}\left[c_{(l,m,k),q} \cdot \cos\left(\frac{2\pi}{L} q\Omega_{coup.} s\right) + d_{(l,m,k),q} \cdot \sin\left(\frac{2\pi}{L} q\Omega_{coup.} s\right)\right], \tag{75}$$

$$\left(l\frac{\partial A_{0,0,0}}{\partial I_x} + m\frac{\partial A_{0,0,0}}{\partial I_z}\right) = \frac{e_{(l,m,k),0}}{2} + \tag{76}$$
$$\sum_{q=1}^{\infty}\left[e_{(l,m,k),q} \cdot \cos\left(\frac{2\pi}{L} q\Omega_{coup.} s\right) + f_{(l,m,k),q} \cdot \sin\left(\frac{2\pi}{L} q\Omega_{coup.} s\right)\right],$$

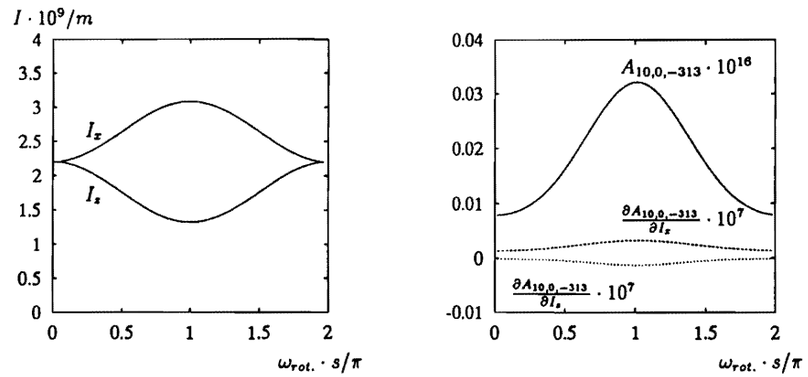

Figure 12: The action oscillations for rotational motion near the coupling resonance for $I_+ = 4.4 \cdot 10^{-9} m$.
Left: The oscillations of the horizontal and vertical actions.
Right: The resulting change in the mode amplitude $A_{10,0,-313}$ and its derivatives with respect to the horizontal and vertical actions.

we get

$$\dot{I}_+ = \varepsilon \cdot \sum_{(l,m,k),\vec{n}_{slow},u} \frac{(l+m)}{2} \cdot \left[\prod_{p=1}^{N} J_{n_{fast,p}}\left(\frac{l\Delta Q_{fast,p}}{\Omega_{fast,p}}\right)\right]\left[\prod_{p=1}^{N} J_{n_{slow,p}}\left(\frac{l\Delta Q_{slow,p}}{\Omega_{slow,p}}\right)\right] \times \tag{77}$$

$$\left\{\hat{b}_{(l,m,k),u} \cdot \cos\left(l\phi_x + m\phi_z + \frac{2\pi}{L}\left(k + \vec{n}_{fast} \cdot \vec{\Omega}_{fast} + \vec{n}_{slow} \cdot \vec{\Omega}_{slow} + u \cdot \Omega_{coup.}\right) s + \delta_{l,k}\right) + \right.$$

$$\left. \hat{a}_{(l,m,k),u} \cdot \sin\left(l\phi_x + m\phi_z + \frac{2\pi}{L}\left(k + \vec{n}_{fast} \cdot \vec{\Omega}_{fast} + \vec{n}_{slow} \cdot \vec{\Omega}_{slow} + u \cdot \Omega_{coup.}\right) s + \delta_{l,k}\right)\right\},$$

with

$$\hat{a}_{(l,m,k),u} = a_{(l,m,k),u} = \hat{a}_{(l,m,k),-u}, \qquad \hat{b}_{(l,m,k),u} = b_{(l,m,k),u} = -\hat{b}_{(l,m,k),-u}. \tag{78}$$

For the zeroth-order solutions of the horizontal angle variables, we get now

$$l\phi_{x,0}(s) + m\phi_{z,0}(s) = (l\nu_x + m\nu_z) \cdot s + \tag{79}$$

$$\frac{L}{2\pi\Omega_{coup.}} \cdot \sum_{q=1}^{\infty}\left[\frac{e_{(l,m,k),q}}{q} \cdot \sin\left(\frac{2\pi}{L} q\Omega_{coup.} s\right) - \frac{f_{(l,m,k),q}}{q} \cdot \cos\left(\frac{2\pi}{L} q\Omega_{coup.} s\right)\right] + l\theta_{x,0} + m\theta_{z,0}.$$

We can insert the first order solution (79) into (77), expand the cosine and sinus terms into a sum of Bessel functions, and integrate the resulting expression over the arc length s. Because the whole procedure involves extremely long expressions, and because the single steps are not very illuminating, we do not present the details of these calculations. Instead, we move

directly to the final expression of the diffusion coefficient. For small amplitudes of the action oscillation, we get for the diffusion coefficient

$$D(I_x, I_z) = \sum_{(l,m,k)} \frac{(l+m)^2\pi}{8l\Delta\nu_x} \cdot \left[\prod_{p=1}^{N} J_{n_{fast,p}}\left(\frac{l\Delta Q_{x,fast}}{\Omega_{fast,p}}\right)\right]^2 \times \tag{80}$$

$$\sum_{u,u'=-\infty}^{+\infty}\left[b_{(l,m,k),u} \cdot b_{(l,m,k),u'} + a_{(l,m,k),u} \cdot a_{(l,m,k),u'}\right] \times$$

$$\sum_{\vec{n}_{slow},\vec{n}'_{slow}} \left\{\left[\prod_{p=1}^{N} J_{n_{slow,p}}\left(\frac{l \cdot \Delta Q_{slow,p}}{\Omega_{slow,p}}\right)\right] \cdot \left[\prod_{p=1}^{N} J_{n'_{slow,p}}\left(\frac{l \cdot \Delta Q_{slow,p}}{\Omega_{slow,p}}\right)\right]\right\},$$

and the corresponding drift coefficient becomes

$$B(I_x, I_z) = \sum_{(l,m,k)} \frac{(l+m)^2\pi}{8l\Delta\nu_x} \cdot \left[\prod_{p=1}^{N} J_{n_{fast,p}}\left(\frac{l\Delta Q_{x,fast}}{\Omega_{fast,p}}\right)\right]^2 \times \tag{81}$$

$$\sum_{u,u'=-\infty}^{+\infty}\left[b_{(l,m,k),u} \cdot \left(\frac{\partial b_{(l,m,k),u'}}{\partial I_x} + \frac{\partial b_{(l,m,k),u'}}{\partial I_z}\right) + a_{(l,m,k),u} \cdot \left(\frac{\partial a_{(l,m,k),u'}}{\partial I_x} + \frac{\partial a_{(l,m,k),u'}}{\partial I_z}\right)\right] \times$$

$$\sum_{\vec{n}_{slow},\vec{n}'_{slow}} \left\{\left[\prod_{p=1}^{N} J_{n_{slow,p}}\left(\frac{l \cdot \Delta Q_{slow,p}}{\Omega_{slow,p}}\right)\right] \cdot \left[\prod_{p=1}^{N} J_{n'_{slow,p}}\left(\frac{l \cdot \Delta Q_{slow,p}}{\Omega_{slow,p}}\right)\right]\right\},$$

where the sums go over all overlaping modulation sidebands with

$$\left(\frac{m}{l}\nu_z + \frac{2\pi}{lL} \cdot \left[\vec{n}_{fast} \cdot \vec{\Omega}_{fast} + (\vec{n}_{slow} - \vec{n}'_{slow}) \cdot \vec{\Omega}_{slow} + (u+u') \cdot \Omega_{coup.} + k\right]\right) \in \tag{82}$$

$$[\nu_x - \Delta\nu_x,\ \nu_x + \Delta\nu_x].$$

If the slow modulation frequencies have no common denominator (68), the sum over the Bessel function of the slow modulation frequencies can be again approximated by one. If we assume further

$$\Delta\nu_x < \frac{2\pi}{L} \cdot \Omega_{coup.}, \tag{83}$$

we get

$$B(I_x, I_z) = \sum_{(l,m,k)} \frac{(l+m)^2\pi}{8l\Delta\nu_x} \cdot \left[\prod_{p=1}^{N} J_{n_{fast,p}}\left(\frac{l\Delta Q_{x,fast}}{\Omega_{fast,p}}\right)\right]^2 \times \tag{84}$$

$$\sum_{u=-\infty}^{+\infty}\left[b_{(l,m,k),u} \cdot \left(\frac{\partial b_{(l,m,k),u}}{\partial I_x} + \frac{\partial b_{(l,m,k),u}}{\partial I_z}\right) + a_{(l,m,k),u} \cdot \left(\frac{\partial a_{(l,m,k),u}}{\partial I_x} + \frac{\partial a_{(l,m,k),u}}{\partial I_z}\right)\right].$$

In the limit of vanishing ΔI_- oscillation amplitudes, only the $u = 0$ Fourier modes are non-zero, and the drift and diffusion coefficients agree with (64), (67), and (69). However, for non-vanishing oscillation amplitudes, Fourier modes with $u \neq 0$ contribute to the drift coefficient. Depending on the initial phase space conditions, the additional contributions due to the ΔI_- oscillation can lead to a drift coefficient that is much larger than the one for a particle motion away from the coupling resonance. For example, for the ΔI_- oscillation in

Fig.12, the drift coefficient is approximately four times larger than the one in the case of no action oscillations. Therefore, the coupling resonance can have a destabilizing effect on the particle motion.

c) If the particles are inside the region of regular motion around the stable fixed points of the coupling resonance, the trapping condition (28) is fulfilled, and the slow tune modulation can not lead to a homogeneous modulational layer. Consequently, the particle motion has no stochastic character, and we expect vanishing drift and diffusion coefficients if the particles are directly on the coupling resonance.

d) For explicitly random tune variations, we have to rewrite the equations of motion to

$$\dot{\phi}_+ = l \cdot (\nu_x + a \cdot \xi) + m \cdot \nu_z \tag{85}$$

$$\dot{I}_+ = \varepsilon \cdot (l+m) \sum_{l,m,k,\vec{n}_{slow}} \bar{A}_{l,m,k,\vec{n}_{fast},\vec{n}_{slow}}(I_x, I_z) \times \tag{86}$$

$$\sin\left(l\phi_x + m\phi_z + \frac{2\pi}{L}\left(k + \vec{n}_{fast} \cdot \vec{\Omega}_{fast} + \vec{n}_{slow} \cdot \vec{\Omega}_{slow}\right) s + \delta_{l,k}\right),$$

where we neglected the coupling mode from the equations of motion, and where ξ is a random function. In the following, we assume that ξ changes its value every τ meter, with $\xi \in [-1, 1]$, $< \xi >= 0$, and $T \leq \tau$. With these assumptions, we can proceed as in the case a) and b), with $\Delta\nu_x = a$. For the particle motion away from the coupling resonance we get for the drift and diffusion coefficients

$$D(I_x, I_z) = \sum_{l,m,k} \frac{(l+m)^2\pi}{2la} \cdot \left[\prod_{p=1}^{N} J_{n_{fast,p}}\left(\frac{l\Delta Q_{fast,p}}{\Omega_{fast,p}}\right)\right]^2 \cdot A^2_{l,m,k}, \tag{87}$$

$$B(I_x, I_z) = \sum_{l,m,k} \frac{(l+m)^2\pi}{2la} \cdot \left[\prod_{p=1}^{N} J_{n_{fast,p}}\left(\frac{l\Delta Q_{fast,p}}{\Omega_{fast,p}}\right)\right]^2 \cdot A_{l,m,k} \cdot \left[\frac{\partial A_{l,m,k}}{\partial I_x} + \frac{\partial A_{l,m,k}}{\partial I_z}\right], \tag{88}$$

and in the case of a particle motion close to the coupling resonance, we get

$$D(I_x, I_z) = \sum_{(l,m,k)} \frac{(l+m)^2\pi}{8la} \cdot \left[\prod_{p=1}^{N} J_{n_{fast,p}}\left(\frac{l\Delta Q_{x,fast}}{\Omega_{fast,p}}\right)\right]^2 \times \tag{89}$$

$$\sum_{u,u'=-\infty}^{+\infty} \left[b_{(l,m,k),u} \cdot b_{(l,m,k),u'} + a_{(l,m,k),u} \cdot a_{(l,m,k),u'}\right],$$

$$B(I_x, I_z) = \sum_{(l,m,k)} \frac{(l+m)^2\pi}{8la} \cdot \left[\prod_{p=1}^{N} J_{n_{fast,p}}\left(\frac{l\Delta Q_{x,fast}}{\Omega_{fast,p}}\right)\right]^2 \times \tag{90}$$

$$\sum_{u=-\infty}^{+\infty} \left[b_{(l,m,k),u} \cdot \left(\frac{\partial b_{(l,m,k),u}}{\partial I_x} + \frac{\partial b_{(l,m,k),u}}{\partial I_z}\right) + a_{(l,m,k),u} \cdot \left(\frac{\partial a_{(l,m,k),u}}{\partial I_x} + \frac{\partial a_{(l,m,k),u}}{\partial I_z}\right)\right].$$

All coefficients do not depend on the correlation time τ and are identical with the coefficients for a purely harmonic tune modulation. Hence, we expect the same diffusion and drift coefficients for an explicitly stochastic tune modulation as in the case of a harmonic tune modulation with the same net rms modulation depth. However, in the limes of vanishing correlation times ($\tau \to 0$), the assumption (63) is not valid and we can not use the results (87), (88), (89), and (90).

We are now ready to discuss the dependence of the drift and diffusion coefficients on the modulation frequencies and depths, and the phase space position. In the next section, we look at different values for the modulation frequencies and compare the analytical estimates for the drift coefficients with tracking data. In all cases, the tracking data turns out to agree qualitatively as well as quantitatively with the analytical estimates in this section.

6 Numerical Results

Before we compare our analytical estimates with tracking data, we will briefly summarize the procedures for the analytical and numerical evaluation of the drift coefficients, and outline the main steps in the comparison of the analytical and numerical results.

We start with the description of the procedure for the analytical estimate. In order to evaluate the amplitudes for the horizontal and vertical action oscillations during the rotational motion, we track one particle with the initial conditions $I_x = I_+/2 = I_z$, $\phi_x \in [-\pi, \pi]$, and $\phi_z = 0$ over 10^4 turns through our model structure. The tracking is done by a successive application of the map (13) to the particle coordinates. The oscillation frequency $\omega_{rot.}$ can be calculated form the linear tunes (46) and has to agree with the value obtained from the particle tracking. Once we know the amplitude ΔI_- and the oscillation frequency $\omega_{rot.}$, we insert the linear solution (47) into the beam-beam potential (2) and use a FFT for the calculation of the Fourier coefficients. Knowing the Fourier coefficients of the mode amplitudes (74), their derivatives (75), and the beam-beam detuning terms (76), we can use (69) or rather (84), for the calculation of the drift coefficient.

For the numerical evaluation of the drift coefficients, we look at a distribution of 3,000 particles and calculate the time evolution of the mean total action by a successive application of the map (13) to the particle coordinates. The mean total action can be calculated from the single particle actions by

$$< I_+ >:= \cdot \sum_{n=1}^{M} \frac{(I_{x,n} + I_{z,n})}{M}, \tag{91}$$

where the summation goes over all particles ($M = 3.000$). (The total emittance is approximately twice the total action.) In order to get reliable numbers for the drift coefficients, we have to follow the particles at least over 10^6 turns. Because of the large number of particles and turns required for reliable tracking results, the numerical evaluation of the drift coefficients is extremely cpu-time consuming. (One point in the Q-diagram needs approximately 1,200 cpu-minutes on an HP 9000-730.)

For a comparison of the analytical estimates and the numerical tracking data, we choose the horizontal linear Q-value

$$Q_x = 31.2971, \tag{92}$$

and look at a Gaussian distribution for the horizontal and vertical actions with

$$< I_y >= \frac{I_+}{2}, \quad \sigma_y = 2.5 \cdot 10^{-10} m, \quad y = x, z, \tag{93}$$

and a uniform distribution of the angle variables

$$\phi_y \in [-\pi, \pi], \quad y = x, z. \tag{94}$$

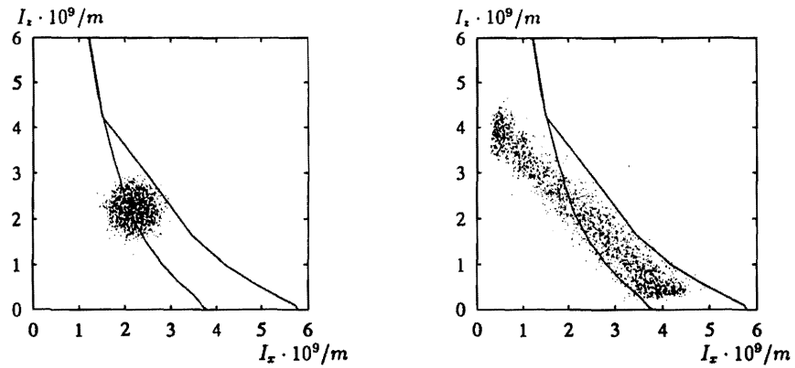

Figure 13:
Left: The initial particle distribution in the transverse action space.
Right: The same particle distribution for a motion on the coupling resonance after 500 turns. Because of the modulation due to the coupling resonance, the particle distribution is subject to an initial spread. In both cases, the external tune modulation was turned off.

The total action corresponds to a normalized emittance of $\epsilon = 2 \cdot I_+ \cdot 874.2$ for $P_0 = 820 GeV/c$. The left-hand side of Fig.13 shows the particle distribution in the transverse action space for horizontal and vertical Q-values away from the coupling resonance, and the right-hand side shows the distribution for Q-values close to the coupling resonance. Both pictures show the particle distribution after 500 turns. Close to the coupling resonance an initial filamentation of the particle distribution due to the motion on the coupling resonance occurs during the first 500 turns. However, this filamentation leads only to an increase of I_-, and not to an increase in the total action I_+. The initial conditions are chosen such that approximately 60% of the particles are on the $1200Hz$ modulation sideband of the purely horizontal 10th order sum resonance. This choice of initial conditions yields approximately the same number of particles inside the modulational layer for all vertical Q-values, and hence, simplifies the comparison of the drift coefficients for different vertical Q-values. The solid lines in Fig.13 show the upper and lower bounds of the modulational layer due to a slow tune modulation with $0.6Hz$ and $\Delta Q_{slow} = 6.25 \cdot 10^{-5}$. For both cases, approximately half the particles are inside the modulational layer. (Without the fast tune modulation, the particles experience no low-order sum resonance, and the diffusion process stops all together.) As we vary the vertical linear Q-value from $Q_z = 32.2962$ to $Q_z = 32.2971$, the particles approach the coupling resonance. Because of the increase in the action oscillations near the coupling resonance, the drift coefficient increases with decreasing distance from the coupling resonance. As the sum resonances start to overlap on the coupling resonance, the contributions of the overlapping resonances add up and lead to an large increase in the drift coefficient (81). If the particle motion takes place inside the region of regular motion around the stable fixed points of the

coupling resonance, the homogeneous modulational layer of the slow tune modulation vanishes and the particle motion has no stochastic character. Consequently, the drift coefficient should vanish for

$$Q_z \in [32.2971 - 0.00025,\ 32.2971 + 0.00025]\,, \tag{95}$$

where we took the width of the coupling resonance from the tracking data (49). For each set of modulation frequencies, we sample the vertical linear Q-value over

$$Q_z \in [32.2962,\ 32,2982]. \tag{96}$$

In the following, we will look at four qualitatively different situations:

a) one fast and one slow modulation frequency:
($f_{fast,1} = 1200Hz, f_{slow} = 0.6Hz$),

b) two fast and one slow modulation frequencies:
($f_{fast,1} = 1200Hz, f_{fast,2} = 50Hz, f_{slow} = 0.6Hz$),

c) two fast, one slow, and one intermediate modulation frequency:
($f_{fast,1} = 1200Hz, f_{fast,2} = 50Hz, f_{slow} = 0.6Hz, f_{int.} = 14.0Hz$),

d) one fast harmonic modulation frequency and one explicitly stochastic modulation signal:
($f_{fast} = 1200Hz, \Delta Q_{stoch.} = 6.25 \cdot 10^{-5}$).

For each case, we calculate upper limits for the $1200Hz$ modulation depth, as it would be required for a large proton lifetime, and look at the dependence of the drift coefficient on the Q-values and the phase space position.

a) We start our discussion with one slow and one fast modulation frequency, and choose

$f_{fast} = 1200Hz$	$\Delta Q_{fast} = 3.13 \cdot 10^{-4}$
$f_{slow} = 0.6Hz$	$\Delta Q_{fast} = 6.25 \cdot 10^{-5}$.

The fast tune modulation might occur in the natural ripple spectrum of the HERA-p power supplies, and the slow tune modulation yields the same order of magnitude for the rms modulation depth as the tune modulation caused by the ground motion in the HERA tunnel [12]. Fig.14 shows the mean total action of the particles versus the number of turns for $Q_z = 32.2971$ and $Q_z = 32.2973$. The numerical data in the left-hand side of Fig.14 confirms the vanishing drift coefficient for a particle motion right on the coupling resonance, and the data in the right-hand side of Fig.14 shows the emittance growth in the direct neighbourhood of the coupling resonance, where all 10th order sum resonances overlap. Fig.15 shows the drift coefficients versus the vertical Q-value. The solid line in Fig.15 shows the analytically calculated drift coefficient for a contribution of the purely horizontal $(10, 0, -313)$ sum resonance alone, and the dashed line shows the analytically calculated drift coefficient for a contribution of all 10th order sum resonances. In the latter, we assumed a symmetrical distribution of the sum resonances around the coupling resonance and in both cases, we assumed that 60% of the particles are inside the modulational layer. For $32.2969 < Q_z < 32.2973$, the particles are inside the region of regular motion around the stable fixed points of the coupling resonance, and the drift coefficients vanish. The squares in Fig.15 show the drift coefficients obtained by the numerical tracking. Away from the coupling resonance, the numerical data agrees nicely with the analytical estimates. As the vertical Q-values approach the coupling

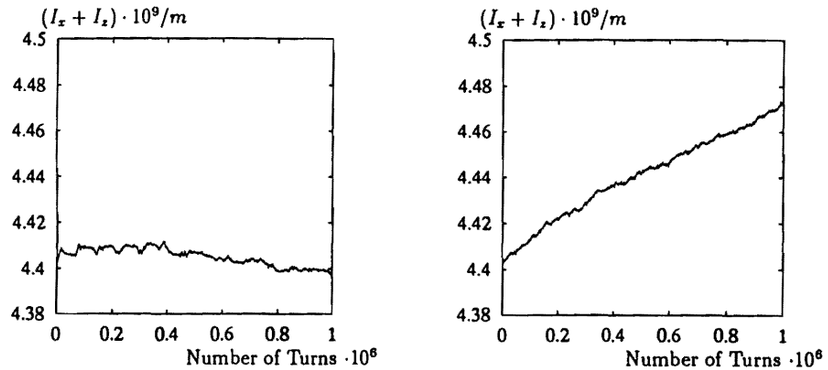

Figure 14:
Left: The mean total action versus the number of turns for $Q_z = 32.2971$.
Right: The mean total action versus the number of turns for for $Q_z = 32.2973$.

resonance ($Q_z = (Q_x + 1) = 32.2971$), the drift coefficient increases. The solid line in Fig.15 shows an increase of the drift coefficient by a factor of two due to the action oscillations close to the coupling resonance. For $32.2965 < Q_z < 32.298$, the numerical data shows an increase of the drift coefficient larger than the one predicted by the horizontal $(10, 0, -313)$ sum resonance alone, indicating an additional contribution of the $(8, 2, -315)$, $(6, 4, -317)$, $(4, 6, -319)$, and $(2, 8, -321)$ sum resonances. The dashed line in Fig.15 shows the drift coefficient for a consideration of all 10th order sum resonances. For vertical Q-values smaller than (32.297), the measured data is slightly lower than the analytical estimate (dashed line), indicating a asymmetric distribution of the sum resonances around the coupling resonance. If we neglect the regular motion on the coupling resonance, we can calculate an upper bound for the drift coefficient. Using equation (84), we obtain

$$B_{max} \approx 1.0 \cdot 10^{-16} m/Turn.$$

In all cases, the drift coefficients are of the same order of magnitude as the ones measured during the 1992 HERA luminosity run [7]

$$B_{HERA} \sim 0.2 \cdot 10^{-16} m/Turn,$$

and are not large enough to spoil the beam lifetime.

This changes if we look at a stronger $1200Hz$ modulation. For

$f_{fast} = 1200Hz$	$\Delta Q_{fast} = 1.25 \cdot 10^{-3}$
$f_{slow} = 0.6Hz$	$\Delta Q_{fast} = 6.25 \cdot 10^{-5}$,

the Bessel functions of the $1200Hz$ modulation in (84) become larger, and the drift coefficient should increase by approximately one order of magnitude. Fig.16 shows the corresponding values for the analytically and numerically calculated drift coefficients.

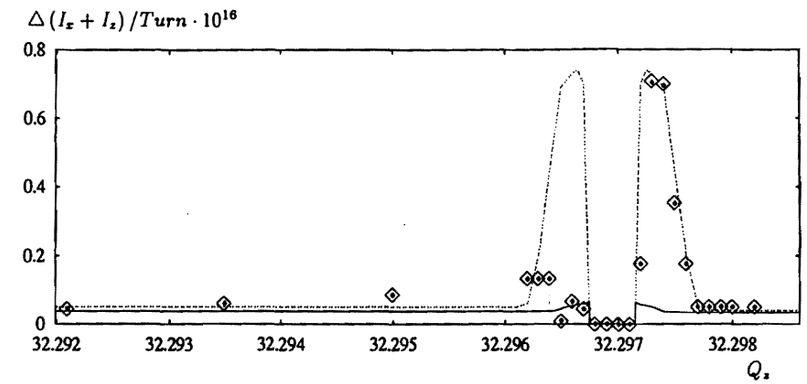

Figure 15: The drift coefficient versus the vertical Q-value for $Q_x = 31.2971$ and a harmonic tune modulation with two frequencies:
$f_1 = 1200Hz, \Delta Q_{1200Hz} = 1.3 \cdot 10^{-4}$ and $f_2 = 0.6Hz, \Delta Q_{0.6Hz} = 6.25 \cdot 10^{-5}$. The solid line shows the analytical estimates for a contribution of the purely horizontal $(10, 0, -313)$ sum resonance alone, the dashed line the drift coefficient for a contribution of all 10th order sum resonances and the squares show the numerically calculated drift coefficients.

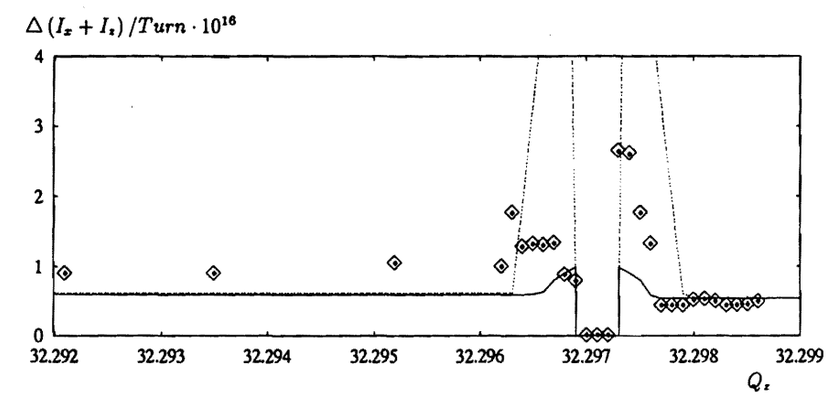

Figure 16: The drift coefficient versus the vertical Q-value for $Q_x = 31.2971$ and a harmonic tune modulation with two frequencies:
$f_1 = 1200Hz, \Delta Q_{1200Hz} = 1.3 \cdot 10^{-3}$ and $f_2 = 0.6Hz, \Delta Q_{0.6Hz} = 6.25 \cdot 10^{-5}$. The solid line shows the analytical estimates for a contribution of the purely horizontal $(10, 0, -313)$ sum resonance alone, the dashed line the drift coefficient for a contribution of all 10th order sum resonances and the squares show the numerically calculated drift coefficients.

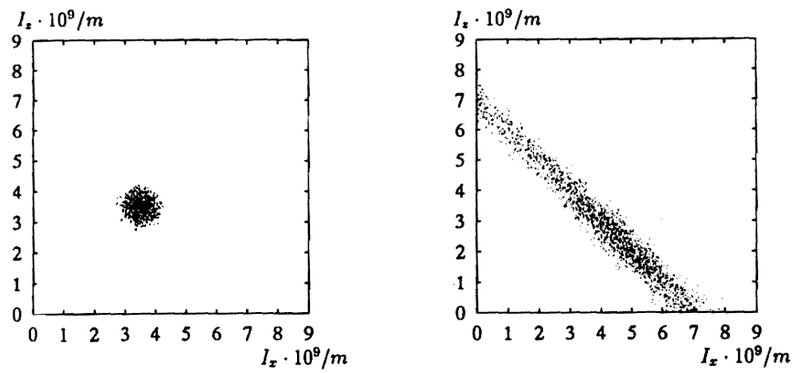

Figure 17:
Left: The initial particle distribution in the transverse action space for case b).
Right: The same particle distribution for a motion on the coupling resonance after 500 turns. Because of the action oscillations near the coupling resonance, the particle distribution is subject to an initial spread. In both cases, the external tune modulation was turned off.

The solid line shows again the analytically calculated drift coefficient for a contribution of the purely horizontal $(10, 0, -313)$ sum resonance alone, the dashed line the drift coefficient for a contribution of all 10th order sum resonances, and the squares the numerically calculated drift coefficients. In the case of a strong $1200Hz$ modulation amplitude, the analytical estimates for a contribution of all 10th order sum resonances are approximately three times larger than the measured data, and approximately one order of magnitude larger than the ones measured in the 1992 HERA luminosity run [7]. For all vertical Q-values, the drift coefficients are large enough to spoil the beam lifetime. Consequently, the tolerances for a $1200Hz$ power supply ripple have to be smaller than $\Delta Q_{1200Hz} = 1.3 \cdot 10^{-3}$. Again, the numerical data shows an increase of the drift coefficient close to the coupling resonance and vanishes directly on the coupling resonance. For $Q_z < 32.2965$, the numerically calculated drift coefficients are always larger than the analytical estimate.

For both $1200Hz$ modulation depths, the coupling mode has a stabilizing as well as a destabilizing effect on the particle motion. The action oscillations outside the regions of regular motion have a destabilizing effect on the particle motion, and the oscillations inside the regions of regular motion have a stabilizing effect. Because of the regions of regular motion around the stable fixed points of the coupling resonance, the particle diffusion vanishes in both cases for $Q_z \approx (Q_x + 1)$.

b Next, we consider two fast and one slow modulation frequencies, and look at a particle distribution on the $(f_1 = 1200Hz, n_1 = 1, f_2 = 50Hz, n_2 = -1)$ sideband of the $(10, 0, -313)$ sum resonance. The left-hand side of Fig.17 shows the particle distribution in the transverse action space for horizontal and vertical Q-values far from the coupling resonance, and the

right-hand side shows the distribution for Q-values close to the coupling resonance. Both pictures show the particle distribution after 500 turns. Close to the coupling resonance, one can observe again an initial filamentation of the particle distribution due to the modulation on the coupling resonance.

We start with the frequencies

$f_{fast,1} = 1200Hz$	$\Delta Q_{fast,1} = 1.25 \cdot 10^{-4}$
$f_{fast,2} = 50Hz$	$\Delta Q_{fast,2} = 4.38 \cdot 10^{-4}$
$f_{slow} = 0.6Hz$	$\Delta Q_{slow} = 6.25 \cdot 10^{-5}$.

With the help of (84), we can calculate upper bounds for the drift coefficients. Away from the coupling resonance, where only the sidebands of the $(10, 0, -313)$ sum resonance contribute, we get

$$B_{th.} \approx 3.0 \cdot 10^{-18} m/Turn,$$

and close to the coupling resonance, where the contribution of all 10th order sum resonances have to be considered, we get

$$B_{th.,max} \approx 0.9 \cdot 10^{-16} m/Turn.$$

Directly on the coupling resonance, the drift coefficient should vanish again because of the regions of regular motion around the stable fixed points of the coupling resonance. The tracking data yields for the average value of the drift coefficient for a particle motion away from the coupling resonance

$$B_{num.} \approx 5.0 \cdot 10^{-18} m/Turn,$$

and a maximum value of

$$B_{num.,max} \approx 0.5 \cdot 10^{-16} m/Turn$$

for $Q_z = 32.2969$. In both cases, the numerical tracking data agrees nicely with the analytical estimates. As expected, the tracking data yields a vanishing drift coefficient for a particle motion on the coupling resonance. In all cases, the drift coefficients are small and do not damage the beam lifetime.

Next, we look at a larger modulation strength for the $1200Hz$ signal

$f_{fast,1} = 1200Hz$	$\Delta Q_{fast,1} = 1.25 \cdot 10^{-3}$
$f_{fast,2} = 50Hz$	$\Delta Q_{fast,2} = 4.38 \cdot 10^{-4}$
$f_{slow} = 0.6Hz$	$\Delta Q_{slow} = 6.25 \cdot 10^{-5}$.

(97)

In this case, the modulational layers of the $50Hz$ sidebands overlap, resulting in one wide modulational layer. Equations (69) and (84) predict an increase in the drift coefficients by almost two orders of magnitude:

$$B_{th.} \approx 5.0 \cdot 10^{-16} m/Turn$$

for a particle motion away from the coupling mode, and

$$B_{th.,max} \approx 5.0 \cdot 10^{-15} m/Turn$$

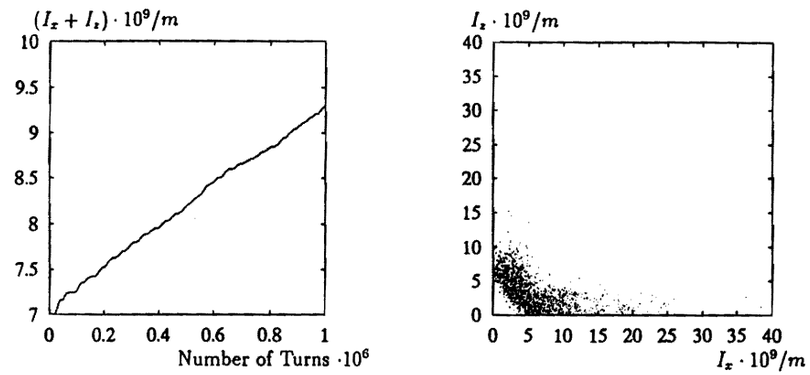

Figure 18:
Left: The mean total action versus the number of turns for $Q_x = 32.2969$ and a tune modulation with:
$f_{fast,1} = 1200Hz, \Delta Q_{fast,1} = 1.25 \cdot 10^{-3}$, $f_{fast,2} = 50Hz, \Delta Q_{fast,2} = 4.38 \cdot 10^{-4}$, and $f_{slow} = 0.6Hz, \Delta Q_{slow} = 6.25 \cdot 10^{-5}$.
Right: The corresponding final particle distribution after 10^6 turns.

for a particle motion in the direct neighbourhood of the coupling resonance. Because the size of the regions of regular motion decreases for the case of overlapping modulational layers, the region of regular motion can not contain the whole particle distribution at once. Hence, one expects the drift coefficients not to vanish for a particle motion on the coupling resonance $Q_z = (Q_x + 1)$, but to attain only a non-vanishing minimum.

The numerical data obtained by the particle tracking confirms the drastic increase of the drift coefficients and the non-vanishing drift coefficient for a particle motion on the coupling resonance. Fig.18 shows the emittance growth for $Q_x = 32.2969$. The left-hand side shows the mean total action versus the number of turns and the right-hand side of Fig.18 shows the corresponding final particle distribution in the transverse action space after 10^6 turns. The numerical data now yields

$$B_{num.} \approx 8.0 \cdot 10^{-16} m/Turn$$

for a particle motion away from the coupling mode, and

$$B_{num.,max} \approx 2.5 \cdot 10^{-15} m/Turn$$

for a particle motion close to the coupling resonance. On the coupling resonance, the tracking data yields

$$B_{num.,coup.} \approx 7.0 \cdot 10^{-16} m/Turn,$$

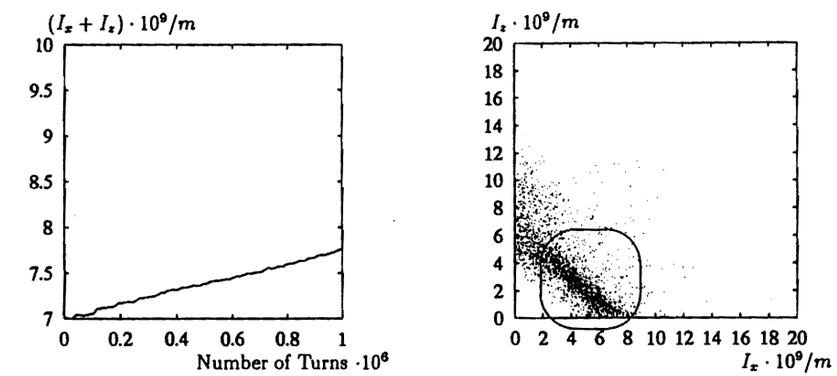

Figure 19:
Left: The mean total action versus the number of turns for $Q_x = 32.2971$ and a tune modulation with:
$f_{fast,1} = 1200Hz, \Delta Q_{fast,1} = 1.25 \cdot 10^{-3}$, $f_{fast,2} = 50Hz, \Delta Q_{fast,2} = 4.38 \cdot 10^{-4}$, and $f_{slow} = 0.6Hz, \Delta Q_{slow} = 6.25 \cdot 10^{-5}$.
Right: The corresponding final particle distribution after 10^6 turns. The oval indicates the particles inside the region of stable motion around the stable fixed points of the coupling resonance.

which is of the same order of magnitude as the drift coefficient for a particle motion away from the coupling mode. The left-hand side of Fig.19 shows the the mean total action versus the number of turns for $Q_x = 32.2971$, and the right-hand side of Fig.19 shows the corresponding final particle distribution after 10^6 turns. In the right-hand side of Fig.19, one can recognize a dark-shaded area, where the particles do not diffuse. This area corresponds to that fraction of the particle distribution which lies inside the region of regular motion. Because the drift coefficient for $Q_x = 32.2971$ is approximately three times smaller than the drift coefficient for $Q_x = 32.2969$, we expect one third of the particle distribution inside the region of regular motion.

For large $1200Hz$ modulation depths, the drift coefficients are large enough to spoil the beam lifetime. Therefore, the tolerances of the power supplies have to be clearly better than (97).

c) Next, we include a tune modulation in the intermediate frequency range ($f \in [10Hz, 50Hz]$) in our analysis. For a tune modulation in the intermediate frequency range, the modulation sidebands of the coupling resonance can overlap in such a way as to lead to a homogeneous modulational layer around the coupling resonance. In that case, the drift coefficient does

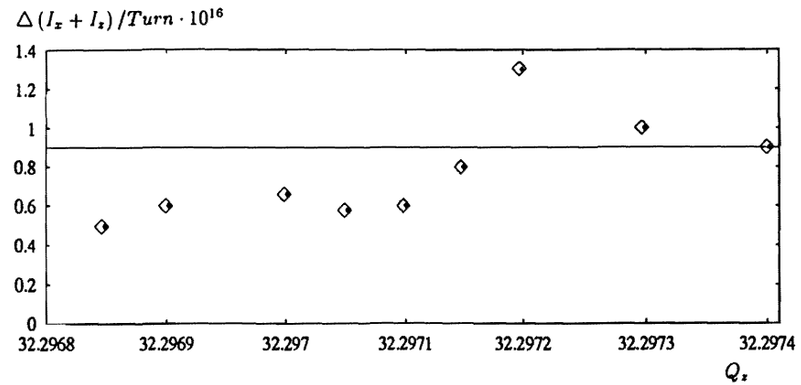

Figure 20: The drift coefficient versus the vertical Q-value for $Q_x = 31.2971$ and a harmonic tune modulation with four frequencies:
$f_1 = 1200Hz, \Delta Q_{1200Hz} = 1.25 \cdot 10^{-4}$, $f_2 = 50Hz, \Delta Q_{50Hz} = 4.38 \cdot 10^{-4}$,
$f_3 = 14Hz, \Delta Q_{14Hz} = 6.25 \cdot 10^{-5}$, and $f_{slow} = 0.6Hz, \Delta Q_{0.6Hz} = 6.25 \cdot 10^{-5}$. The solid line shows the analytical estimate and the squares show the numerically calculated drift coefficients.

not vanish for $(Q_z = (Q_x + 1))$, and the coupling resonance has no stabilizing effect on the particle motion. Because all 10th order sum resonances contribute to the drift coefficient for $(Q_z = (Q_x + 1))$, we expect a large drift coefficient in the direct neighbourhood of the coupling resonance. For

$f_{fast,1} = 1200Hz$	$\Delta Q_{fast,1} = 2.5 \cdot 10^{-4}$
$f_{fast,2} = 50Hz$	$\Delta Q_{fast,2} = 4.38 \cdot 10^{-4}$
$f_3 \in [10Hz, 50Hz]$	$\Delta Q_3 = 6.25 \cdot 10^{-4}$
$f_{slow} = 0.6Hz$	$\Delta Q_{slow} = 6.25 \cdot 10^{-5}$.

(98)

the overlap condition (26) indicates an overlap of the sidebands around the coupling resonance for $(f_3 < 16Hz)$, and the trapping condition (28) indicates a particle trapping for $(f_3 < 1.2Hz)$. Hence, we expect a homogeneous modulational layer around the coupling resonance for an additional tune modulation with

$$1.2Hz < f_3 < 16Hz, \qquad \Delta Q_3 = 6.25 \cdot 10^{-5}.$$

In the following, we look at an additional tune modulation with

$$f_3 = 14Hz, \qquad \Delta Q_3 = 6.25 \cdot 10^{-5}. \tag{99}$$

In this case, the analytical estimate for the drift coefficient on the coupling resonance yields

$$B_{th.,max} \approx 9.0 \cdot 10^{-17} m/Turn,$$

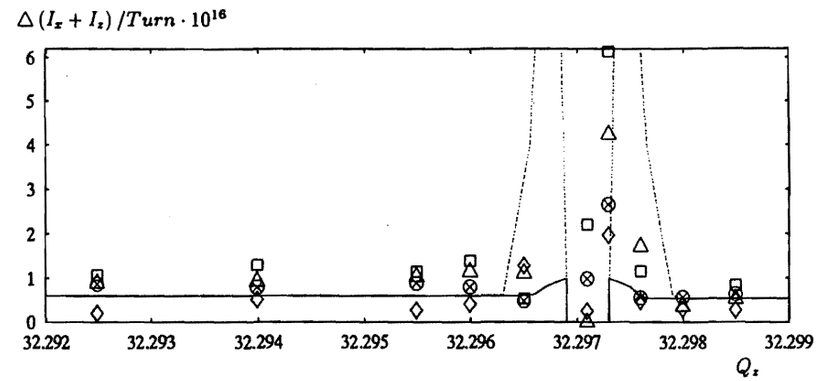

Figure 21: The drift coefficient versus the vertical Q-value for $Q_x = 31.2971$ and a harmonic fast tune modulation with $f_1 = 1200Hz, \Delta Q_{1200Hz} = 1.3 \cdot 10^{-3}$ and an explicitly random tune modulation with $\Delta Q_{stoch.} = 6.25 \cdot 10^{-5}$. The figure shows the numerically calculated drift coefficients for four different correlation times τ:
$\Diamond : \tau = 10^2 \cdot L$, $\square : \tau = 10^3 \cdot L$, $\otimes : \tau = 10^4 \cdot L$, $\triangle : \tau \in [0.2 \cdot 10^4 \cdot L,\ 1.8 \cdot 10^4 \cdot L]$.
In all cases, we looked at the same set of vertical Q-values. The solid line shows the analytical estimates for a contribution of the purely horizontal $(10, 0, -313)$ sum resonance alone, and the dashed line the drift coefficient for a contribution of all 10th order sum resonances.

where we considered the contribution of all 10th order sum resonances and assumed that 60% of the particles are inside the modulational layers. The solid line in Fig.20 shows the corresponding analytical estimate for the drift coefficient and the squares show again the numerically estimated drift coefficients. One clearly recognizes the non-vanishing drift coefficient around the coupling resonance and the nice correspondence of the numerical and analytical data.

d) In a last step, we look at an explicitly random tune modulation. In order to compare the drift coefficients for the explicitly random excitation with the ones for a harmonic slow tune modulation, we look at a fast harmonic tune modulation with the same values as in case a) and replace the slow modulation frequency by a random signal with the same net modulation depth:

$f_{fast} = 1200Hz$	$\Delta Q_{fast} = 1.25 \cdot 10^{-3}$
$a = \frac{2\pi}{L} \cdot \Delta Q_{rand}$	$\Delta Q_{rand.} = 6.25 \cdot 10^{-5}$.

In the following, we will vary the correlation time τ of the random signal in (85) over three orders of magnitude from $[\tau = 10 \cdot L]$ to $[\tau = 10^4 \cdot L]$, and look at constant as well as stochastically varying correlation times τ. The correlation time τ determines the time interval during which the detuning remains constant. As in (85), we assume that the tune changes its value randomly every τ turns within the interval $\nu \in [\nu_x - a,\ \nu_x + a]$ and with $< \nu >= \nu_x$. Fig.21 shows the analytical and numerical estimates for the corresponding drift coefficients versus

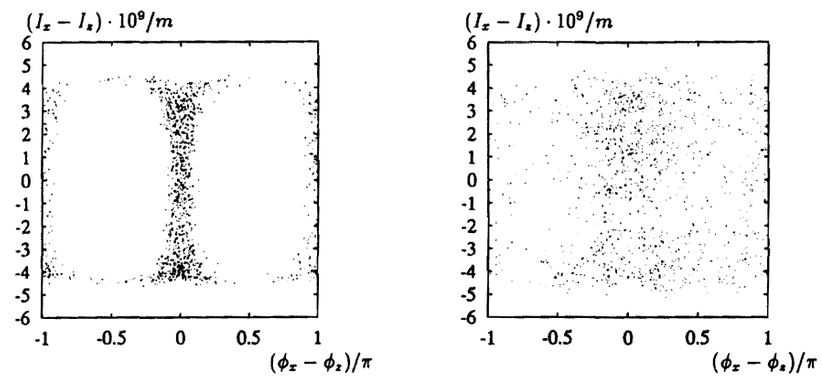

Figure 22: The stroboscobic phase space projection for a particle motion on the coupling resonance and a harmonic as well as random tune modulation with:
$f_{fast} = 1200Hz$, $\Delta Q_{1200Hz} = 1.25 \cdot 10^{-3}$, $\Delta Q_{rand.} = 6.25 \cdot 10^{-5}$.
Left: The projection of $(I_x - I_z)$ and $(\phi_x - \phi_z)$ for a correlation time $\tau = 10 \cdot L$.
Right: The projection of $(I_x - I_z)$ and $(\phi_x - \phi_z)$ for $\tau = 10^3 \cdot L$.

the vertical Q-value. (The horizontal Q-value was again kept constant at $Q_x = 31.2971$.)

The analysis in the previous section showed that the diffusion and drift coefficients caused by an isolated sum resonance and an explicitly random tune modulation are independent from the correlation time τ and reproduce the values obtained for a diffusion due to the stochastic character of the motion inside the modulational layer of a slow harmonic tune modulation. The solid line in Fig.21 shows the analytical estimates of the drift coefficients for a contribution of the purely horizontal $(10, 0, -313)$ sum resonance alone and the dashed line the drift coefficient for a contribution of all 10th order sum resonances. The lines are identical to the lines in Fig.16, where we considered the same fast tune modulation and a harmonic slow tune modulation with $\Delta Q_{slow} = 6.25 \cdot 10^{-5}$. The diamonds show the numerically estimated drift coefficient for $\tau = 10^2 \cdot L$, the squares the numerical values for $\tau = 10^3 \cdot L$, the circles the values for $\tau = 10^4 \cdot L$, and the triangles the values for a randomly changing correlation time. Away from the coupling resonance, the numerical data is independent from the correlation time τ, and agrees nicely with the analytical estimates. Away from the coupling resonance, only the purely horizontal sum resonance sideband contributes to the diffusion and the drift coefficient does not vary with the vertical Q-value and the correlation time τ.

As in the case of a purely harmonic tune modulation, all 10th order sum resonances contribute to the particle diffusion for $(Q_x - Q_z = -1)$, and the drift coefficient attains its maximum value for a particle motion close to the coupling resonance. While the drift coefficient remains constant for a particle motion away from the coupling resonance, the drift coefficient for a particle motion near the coupling resonance changes with τ and Q_z. De-

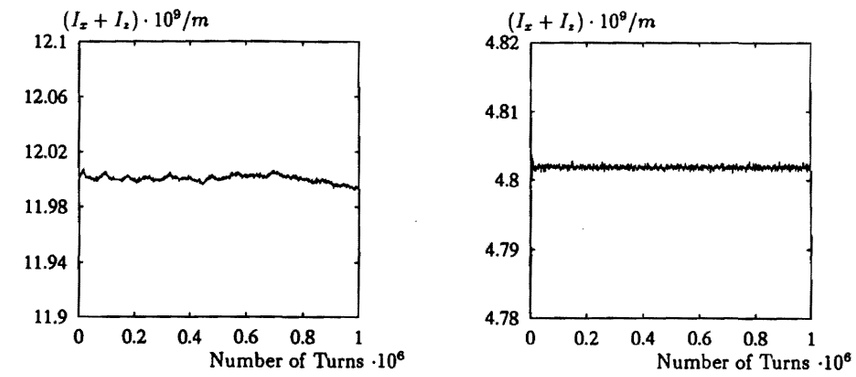

Figure 23: Purely harmonic tune modulation with fast and slow frequency components:
Left: The mean total action versus the number of turns for an initial particle distribution outside the modulational layer.
Right: The mean total action versus the number of turns for a tune modulation without the fast $1200Hz$ component.
In both cases, the total action remains constant.

pending on the correlation time τ, regions of regular motion around the stable fixed points of the coupling resonance can limit the particle diffusion. Fig.22 shows a stroboscobic phase space projection of $(I_x - I_z)$ and $(\phi_x - \phi_z)$ for a particle motion on the coupling resonance. The left-hand side of Fig.22 shows the projection for $\tau = 10 \cdot L$. One clearly recognizes the regions of regular motion around the stable fixed points of the coupling resonance. The right-hand side of Fig.22 shows the stroboscobic phase space projection for $\tau = 10^3 \cdot L$. Here, the particle motion spreads uniformly over the whole range of $(\phi_x - \phi_z)$ and experiences no regions of regular motion. For $\tau = 10 \cdot L$ the regions of regular motion around the stable fixed points of the coupling resonance capture the particles on the coupling resonance and lead to a vanishing drift coefficient (The circles in Fig.fdiff3 show the vanishing drift coefficient for $(Q_z = Q_x + 1)$.) For $\tau = 10^3 \cdot L$ the regions of regular motion disappear and the drift coefficient attains a non-vanishing value on the coupling resonance. Hence, the maximum value of the drift coefficient near the coupling resonance depends on the correlation time τ.

At the end of this section, we want to underline the 'local' character of the particle diffusion in the case of only one fast modulation frequency. In all the above cases, particle diffusion is caused by a simultaneous tune modulation with fast and slow frequency components. If we turn off the slow or the fast tune modulation, or if we look at a particle distribution outside the modulational layer, we do not observe any particle diffusion. The left-hand side of Fig.23 shows the mean total action versus the number of turns for a particle distribution with

$$< I_y >= 6.0 \cdot 10^{-9} m, \quad \sigma_y = 2.5 \cdot 10^{-10} m, \quad y = x, z,$$

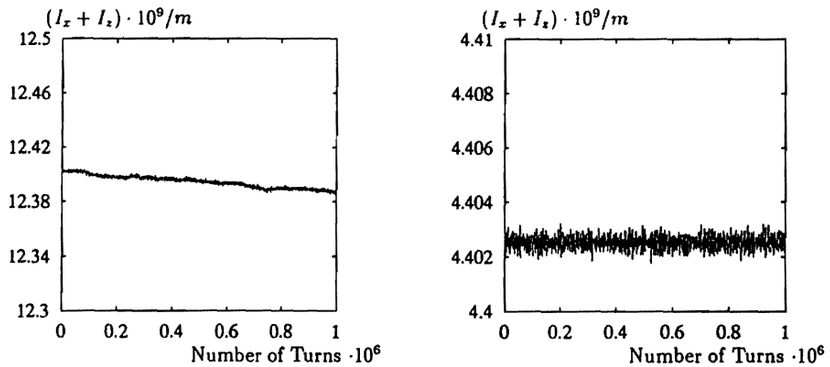

Figure 24: Harmonic as well as random tune modulation: ($\tau = 10^3 \cdot L$), $\Delta Q_{rand} = 6.25 \cdot 10^{-5}$.
Left: The mean total action versus the number of turns for an initial particle distribution outside the modulational layer and a harmonic tune modulation with $f_{fast} = 1200Hz$, $\Delta Q_{1200Hz} = 1.25 \cdot 10^{-3}$.
Right: The mean total action versus the number of turns for a random tune modulation without the fast $1200Hz$ component.
In both cases, the total action remains constant.

$$Q_x = 31.2971, \qquad Q_z = 32.2971,$$

and a tune modulation with

$f_{fast} = 1200Hz$	$\Delta Q_{fast} = 1.25 \cdot 10^{-3}$
$f_2 = 14Hz$	$\Delta Q_2 = 3.13 \cdot 10^{-5}$
$f_{slow} = 0.6Hz$	$\Delta Q_{slow} = 6.25 \cdot 10^{-5}$.

Because the total emittance is more than twice as large as in case b), the initial particle distribution does not lie inside the modulational layer of the $1200Hz$ sideband, and the total action remains constant. Fig.11 shows the position of the $1200Hz$ sideband in the transverse action space. The right-hand side of Fig.23 shows the mean total action versus the number of turns for a particle distribution with

$$< I_y >= 2.4 \cdot 10^{-9}m, \quad \sigma_y = 2.5 \cdot 10^{-10}m, \quad y = x, z,$$

$$Q_x = 31.2971, \qquad Q_z = 32.2971,$$

and a tune modulation with

$f_{fast} = 1200Hz$	$\Delta Q_{fast} = 0.0$
$f_2 = 14Hz$	$\Delta Q_2 = 3.13 \cdot 10^{-4}$
$f_{slow} = 0.6Hz$	$\Delta Q_{slow} = 6.25 \cdot 10^{-5}$.

Because the tune modulation has no $1200Hz$ component, the particles are once again not inside a modulational layer and the total action remains constant.

Both examples illustrate the local aspect of the particle diffusion. The particle diffusion due to a harmonic tune modulation with fast and slow frequency components occurs only for particles inside the modulational layer. A similar statement applies for the simultaneous tune modulation with a fast harmonic frequency and an explicitly random signal. Even in the case of an explicitly random tune modulation, the diffusion stops once we turn off the fast $1200Hz$ modulation, or if the particles are in a phase space area where they can not reach any sum resonance sidebands.. The left-hand side of Fig.24 shows the mean total action ($I_+ = I_x + I_z$) versus the number of turns through the model structure for a particle distribution away from the 10th order sum resonance sidebands:

$$< I_y >= 6.2 \cdot 10^{-9}m, \quad \sigma_y = 2.5 \cdot 10^{-10}m, \quad y = x, z,$$

$$Q_x = 31.2971, \qquad Q_z = 32.2971.$$

The right-hand side of Fig.24 shows the mean total action versus the number of turns for the case of a purely random tune modulation without any harmonic fast tune modulations and

$$< I_y >= 2.4 \cdot 10^{-9}m, \quad \sigma_y = 2.5 \cdot 10^{-10}m, \quad y = x, z,$$

$$Q_x = 31.2971, \qquad Q_z = 32.2940.$$

In both cases the tunes were As in the previous two examples for a purely harmonic tune modulation, the diffusion stops once the particles can not experience a sum resonance sideband. Only for modulation depths large enough for the particles to cross a sum resonance, the particles diffuse in the transverse action space.

Hence, assuming moderate modulation depths for the slow tune modulation and only one fast modulation frequency, one can generate modulational layers which influence only the particle motion inside the beam halo. For appropriate choices of the fast modulation frequencies, such a local diffusion causes a slow emittance growth in the beam halo and might be relevant for a parasitic experiment such as the proposed HERA-B experiment in HERA-p [9].

7 Summary

Looking at a simple model structure for the HERA proton storage ring, we analyzed the emittance growth due to the combined effect of the beam-beam nonlinearities and a harmonic tune modulation with more than one frequency. The model structure consists of six transfer maps for the linear motion and a harmonic tune modulation with up to four modulation frequencies, and two beam-beam kicks in the weak strong approximation. In all cases, we looked at a working point close to the coupling resonance and located between the 7th and 10th order sum resonances, as it was used in the 1992 HERA luminosity run. We used the modulational diffusion [8][4] for a quantitative analysis of the emittance growth due to the tune modulation and derived analytical expressions for the diffusion and drift coefficients.

The analysis demonstrated that a simultaneous tune modulation with more than one frequency leads to a much larger emittance growth than in the case of a tune modulation with only one frequency but the same net modulation depth. A harmonic tune modulation with

fast and slow frequency components causes a particle diffusion of the same order of magnitude as the one measured in a real storage ring. Depending on the modulation frequencies, the diffusion occurs over a wide range of the transverse Q-values and is strong enough to limit the beam lifetime.

In three examples for the frequency spectrum of the power supply ripple, we showed how one can use the analytical expressions for the diffusion and drift coefficients for an estimate of the maximum modulation depths compatible with a large beam lifetime. To this end, we examined a constant total rms modulation depth for the slow tune modulation, as it might occur due to the ground motion in the HERA tunnel ($\Delta Q_{rms} \approx 3 \cdot 10^{-5}$), and used only the modulation depths of the fast tune modulations as free parameters. In all examples, the analytical estimates agreed qualitatively as well as quantitatively with the tracking data and could be used for a calculation of the ripple tolerances in the power supplies. The results show that the ripple tolerances not only depend on the total rms modulation strength of the fast modulation frequencies, but also on the frequency spectrum of the power supply ripples.

In the case of only one fast modulation frequency, the particle diffusion has a local character. Depending on the modulation frequencies, depths, and the tune values, the particle diffusion occurs only in specific regions of the accessible phase space. This type of local particle diffusion could be used for the generation of a slow emittance growth in the beam halo, and might be relevant for a parasitic experiment such as the proposed HERA-B experiment[9]. However, in the presence of more than one fast modulation frequency with non-neglegible modulation amplitudes, the local aspect of the particle diffusion disappears and the emittance growth occurs over large areas of the phase space.

References

[1] O. Brüning (DESY),
Particle Accelerators **41**, pp 133-151 (1993)

[2] X.Altuna, C.Arimatea, R.Bailey, T.Bohl, D.Bramdt, K.Cornelis, C.Depas, F.Galluccio, J.Gareyte, R.Giachino, M. Giovannozzi, Z.Guo, W.Herr, A.Hilaire, T.Lundberg, J.Miles, L.Normann, T.Risselada, W.Scandale, F.Schmidt, A.Spinks, M.Venturini,
CERN SL/91-43 (AP), LHC Note 171, (1991)

[3] O. Brüning (DESY),
DESY HERA 93-05 (May 1993)

[4] A.J. Lichtenberg and M.A. Lieberman,
'Regular and Stochastic Motion', Springer

[5] B.V. Chirikov,
Physics Reports **52**, 263-379 (1979)

[6] R. Brinkmann (DESY),
DESY HERA 89-24 (November 1989)

[7] M. Seidel,
DESY HERA 93-04 (April 1993)

[8] B.V. Chirikov, M.A.Lieberman, D.L.Shepelyansky and F.M.Vivaldy,
Physica **14D**, (1985), 289-304

[9] Letter of Intent,
DESY-PRC 92/04 (October 1992)

[10] R.Bacher, R.Lange, K.-H.Meß, M.Seidel,
DESY HERA 90-16 (September 1990)

[11] O. Brüning (DESY),
In 'Bad Lauterberg 1992, Proceedings, Harz Seminar', 411-419

[12] W. Decking (DESY),
DESY HERA 90-13 (August 1990)

[13] F. Willeke and G. Ripken,
DESY 88-114 (August 1988)

[14] H. Mais,
DESY-PRC 92/04 (October 1991)

[15] A. Deprit,
Cel. Mech. 1,12 (1969)

[16] K. Flöttmann (DESY),
DESY HERA 90-09 (August 1990)

[17] J.L.Tennison, M.A.Lieberman, and A.J.Lichtenberg,
In M.Month and J.C.Herrera (eds.)
'Nonlinear Dynamics and the Beam-Beam Interaction',
AIP Conference Proceedings **57**(p.158)

[18] V.I. Arnold, Russian Mathematical Surveys 18 (1973) 85.

[19] B.V. Chirikov and D.L. Shepelyansky,
Preprint 81-69,
Institute of Nuclear Physics, Novosibirsk (1981),
PPPL Trans. 133, Princeton (1983)

[20] L.R.Evans, J.Gareyte, 'The Beam-Beam Effect in the SPS',
CERN SPS/82-8(DI-MST) (1982)

[21] L.R.Evans, 'The Beam-Beam Interaction'
CERN Accelerator School 'Antiprotons in Colliding Beam Fascilities'
Geneva 1984, CERN 84-15(1984)

[22] M. Abramowitz, A. Stegun,
'Pocketbook of Mathematical Functions', Verlag Harri Deutsch